

1 **Multi-model Estimates of Intercontinental Source-Receptor Relationships for Ozone**
2 **Pollution**

3
4 A.M. Fiore¹, F.J. Dentener², O. Wild³, C. Cuvelier², M.G. Schultz⁴, P. Hess⁵, C. Textor^{6,7},
5 M. Schulz⁷, R. Doherty⁸, L.W. Horowitz¹, I.A. MacKenzie⁸, M.G. Sanderson⁹, D.T.
6 Shindell¹⁰, D.S. Stevenson⁸, S.Szopa⁷, R.Van Dingenen², G. Zeng¹¹, C. Atherton¹², D.
7 Bergmann¹², I.Bey¹³, G. Carmichael¹⁴, B.N. Duncan¹⁵, G. Faluvegi¹⁰, G. Folberth¹³, M.
8 Gauss¹⁶, S. Gong¹⁷, D. Hauglustaine⁷, T. Holloway¹⁸, I.S.A. Isaksen¹⁶, D.J. Jacob¹⁹, J.E.
9 Jonson²⁰, J. W. Kaminski²¹, T.J. Keating²², A. Lupu²¹, E. Marmer², V. Montanaro²³, R.
10 Park^{19,24}, G. Pitari²³, K.J. Pringle^{9,25}, J.A. Pyle¹¹, S. Schroeder⁴, M.G.Vivanco²⁶, P.
11 Wind²⁰, G. Wojcik²⁷, S. Wu¹⁹, A. Zuber²⁸

- 12
13 1. Geophysical Fluid Dynamics Laboratory, NOAA, Princeton, NJ, USA.
14 2. European Commission, DG-Joint Research Centre, Institute for Environment and
15 Sustainability, Ispra, Italy.
16 3. Department of Environmental Science, Lancaster University, UK.
17 4. ICG-2, Forschungszentrum-Jülich, Germany.
18 5. National Center for Atmospheric Research, Boulder, CO, USA.
19 6. Service d'Aéronomie, CNRS/UPMC/IPSL, Paris, France.
20 7. Laboratoire des Science du Climat et de l'Environnement, Gif-sur-Yvette, France.
21 8. School of GeoSciences, University of Edinburgh, UK.
22 9. Met Office Hadley Centre, Exeter, UK.
23 10. NASA Goddard Institute for Space Studies and Columbia University, New York, NY,
24 USA.
25 11. National Centre for Atmospheric Science, Department of Chemistry, University of
26 Cambridge, UK
27 12. Atmospheric Science Division, Lawrence Livermore National Laboratory, CA, USA.
28 13. EPFL, Lausanne, Switzerland.
29 14. Center for Global and Regional Environmental Research, University of Iowa, Iowa
30 City, IA, USA.
31 15. Goddard Earth Sciences & Technology Center, UMBC, MD, USA.
32 16. Department of Geosciences, University of Oslo, Norway.
33 17. Science and Technology Branch, Environment Canada, Toronto, Canada
34 18. Center for Sustainability and the Global Environment, University of Wisconsin-
35 Madison, Madison, WI, USA.
36 19. Atmospheric Chemistry Modeling Group, Harvard University, Cambridge, MA,
37 USA.
38 20. Norwegian Meteorological Institute, Oslo, Norway.
39 21. Center for Research in Earth and Space Science, York University, Canada.
40 22. Office of Policy Analysis and Review, Environmental Protection Agency,
41 Washington DC, USA.
42 23. Dipartimento di Fisica, Università de L'Aquila, Italy
43 24. Now at Seoul National University, Korea.
44 25. Now at Max Planck Institute for Chemistry, Mainz, Germany.
45 26. CIEMAT, Madrid, Spain.
46 27. Northrop Grumman Corporation, VA, USA.

47 28. Environment Directorate General, European Commission, Brussels, Belgium.

48

49 Index Terms:

50 0368 Troposphere: constituent transport and chemistry

51 0478 Pollution: urban, regional and global

52 0345 Pollution: urban and regional

53 3300 ATMOSPHERIC PROCESSES

54 6620 Science policy

55

56 Running Title: Hemispheric Transport of Ozone Pollution

57

58 Keywords: surface ozone, intercontinental transport, methane

59

60 **Abstract**

61

62 A thorough understanding of the surface O₃ response over a “receptor” region to
63 emission changes over a foreign “source” region is needed to evaluate the potential gains
64 from an international approach to abate ozone (O₃) pollution. We apply an ensemble of
65 21 global and hemispheric chemical transport models to estimate the average surface O₃
66 response over East Asia (EA), Europe (EU), North America (NA) and South Asia (SA) to
67 20% decreases in anthropogenic emissions of the O₃ precursors, NO_x, NMVOC, and CO
68 (individually and combined), from each of these regions. The ensemble mean O₃
69 matches observed surface concentrations throughout the year over EU but overestimates
70 them by >10 ppb during summer and early fall over NA and EA. The sum of the O₃
71 responses to NO_x, CO, and NMVOC perturbations is approximately equal to that with all
72 three precursors reduced together, and we focus here on the response to combined
73 reductions. The most robust annual mean responses across the models are that surface O₃
74 concentrations over EU are most influenced by anthropogenic emissions reductions over
75 NA (ensemble mean: 0.4 ppb; inter-model range: 0.2-0.5 ppb), and that emissions
76 reductions over SA have the smallest effect on the other receptor regions (< 0.2 ppb).
77 Emission reductions in the three foreign regions decrease annual mean surface O₃ over
78 the Asian regions by 0.2-0.4 ppb each, and reductions in EA and EU decrease annual
79 mean O₃ by 0.2 ppb each over NA, although the relative impacts vary by model.
80 Applying these ensemble annual mean results to changes in anthropogenic emissions
81 from 1996 to 2002, we estimate a Northern Hemispheric increase in background surface
82 O₃ of about 0.1 ppb yr⁻¹, at the low end of the 0.1-0.5 ppb yr⁻¹ derived from observations.
83 The ensemble mean surface O₃ response to emission reductions in the 3 foreign regions
84 combined is largest in spring and late fall (~0.8 ppb in all regions). We define an “import
85 sensitivity” to gauge the relative contribution of foreign versus “domestic” (*i.e.*, over the
86 source region itself) emission changes for each region. This ratio ranges from 0.5 to 1.1
87 during the months of maximum foreign influence, and from 0.2 to 0.5 when domestic
88 influence is largest. From an additional simulation in which global atmospheric methane
89 was reduced, we infer that 20% reductions in regional anthropogenic methane emissions
90 would yield an O₃ response over foreign receptor regions roughly equal to that produced
91 by 20% reductions of anthropogenic NO_x, NMVOC and CO emissions.

92

93 1. Introduction

94
95 Reducing aerosol and ozone (O₃) levels in surface air is desirable for improving
96 public health as exposure to these atmospheric constituents aggravates respiratory illness
97 and may lead to premature mortality [World Health Organization, 2005]. Findings from
98 numerous observational and modeling studies indicate that long-range transport of
99 pollutants degrade air quality over remote continents [e.g., Wilkening et al., 2000;
100 Holloway et al., 2003; Akimoto et al., 2003]. Satellite images of aerosols, particularly
101 dust and smoke, illustrate the capacity for dust storms and biomass burning to influence
102 tropospheric composition on a hemispheric scale [e.g., Husar et al., 2001]. Ground-
103 based measurements of aerosol composition provide evidence for a foreign influence in
104 surface air; for example, the presence of smoke from Siberian fires and dust from Asia
105 and Africa over the United States [e.g., Prospero, 1999; Jaffe et al., 2003a, 2004]. In
106 contrast, attributing O₃ pollution to a specific source region is complicated by the
107 interplay of processes influencing intercontinental transport (export from the source
108 region, non-linear chemical processing and dilution in transit, and mixing with surface air
109 over the receptor region), and by a large hemispheric background and the dominance of
110 local emissions in contributing to high-O₃ events [e.g., Derwent et al., 2003; Fiore et al.,
111 2003; Goldstein et al., 2004; Jonson et al., 2005]. Given the difficulty of diagnosing O₃
112 source-receptor (SR) relationships (i.e., the change in O₃ over a receptor region produced
113 by emission changes within a source region) from observations, estimates of these
114 relationships rely heavily on models. Here, we use an ensemble of 21 global and
115 hemispheric chemical transport models (CTMs; Table A1) to quantify the impact of O₃
116 precursor emissions from four major continental-scale source regions in the Northern
117 Hemisphere on surface O₃ in the same four “receptor” regions (Figure 1). Prior studies
118 indicate that multi-model mean results better represent a range of observations than any
119 individual model [Schulz et al., 2006; Stevenson et al., 2006; Reichler and Kim, 2008];
120 the range of results across individual models further provides a measure of uncertainty in
121 our understanding as represented in the current generation of CTMs.

122 Tropospheric O₃ is produced via the photochemical oxidation of volatile organic
123 compounds (VOC) and carbon monoxide (CO) in the presence of nitrogen oxides (NO_x).
124 To date, regulations to abate surface O₃ pollution address emissions of the traditional O₃
125 precursors (NO_x, non-methane VOC and CO) which react within hours-to-weeks to
126 produce a “short-term” O₃ response. By altering hydroxyl radical (OH) concentrations,
127 perturbations to emissions of these species affect the major loss pathway for methane
128 (CH₄), the most abundant atmospheric VOC and a major precursor to O₃ in the remote
129 troposphere [Crutzen, 1973; Prather, 1996; Daniel and Solomon, 1998; Fuglestvedt et
130 al., 1999; Derwent et al., 2001; Collins et al., 2002], producing a “long-term” influence
131 on surface O₃. This “long-term” O₃ response follows the time scale and the spatial
132 pattern of the O₃ production from CH₄, and somewhat offsets the O₃ response to
133 perturbations in surface NO_x emissions, while enhancing the response to NMVOC and
134 CO emission changes. [Wild et al, 2001; West et al., 2007]. Anthropogenic CH₄
135 emissions have also been shown to contribute directly to O₃ in surface air [Fiore et al.,
136 2002a; Dentener et al., 2005; West et al., 2007; Fiore et al., 2008]. The contributions to
137 surface O₃ over a receptor region both from CH₄ and from the foreign emissions of the
138 traditional O₃ precursors are generally considered to be part of the “background” O₃ level

139 (along with natural precursor emissions), and are not generally considered in air pollution
140 mitigation strategies.

141 Analysis of observations at northern mid-latitudes indicate that background O₃
142 has been increasing in recent years, although estimates vary, with some revealing little
143 change [e.g., Vingarzan, 2004; TF HTAP, 2007; Oltmans et al., 2006; Derwent et al.,
144 2007; Schultz et al., 2007]. Several modeling studies suggest that projected increases in
145 emissions around the globe will enhance hemispheric background O₃ in the coming
146 decades, potentially offsetting efforts to improve regional air quality via controls on
147 domestic precursor emissions [e.g. Jacob et al., 1999; Yienger et al., 2000; Collins et al.,
148 2000; Fiore et al. 2002a; Dentener et al., 2005; Derwent et al., 2006; Szopa et al., 2006;
149 Ellingsen et al., 2008]. Efforts to improve air quality typically focus on controlling local
150 and regional sources. In nations where O₃ precursors have been regulated for decades,
151 the combination of increasing hemispheric background levels and mounting control costs
152 could make pursuing international cooperation an attractive option [Keating et al., 2004;
153 Bergin et al., 2005; Solberg et al., 2005]. An international approach to air quality
154 management will require a strong scientific understanding of the SR relationships
155 between continents and nations.

156 Under the United Nations Economic Commission for Europe (UNECE)
157 Convention on Long Range Transboundary Air Pollution (CLRTAP), the Task Force on
158 Hemispheric Transport of Air Pollution (TF HTAP; www.htap.org) was established to
159 advance the understanding of hemispheric transport of air pollutants in the Northern
160 Hemisphere. A major TF HTAP activity is to coordinate a multi-model effort to quantify
161 and estimate uncertainties in intercontinental SR relationships for O₃, aerosols, mercury,
162 and persistent organic pollutants. Companion manuscripts investigate NO_y deposition
163 [Sanderson et al., 2008], transport with idealized tracers [Schultz et al, 2008, in prep], the
164 Arctic as a receptor region [Shindell et al, 2008], and aerosols [Schulz et al, 2008, in
165 prep].

166 Prior estimates for intercontinental SR relationships differ by factors of about 2 to
167 6 for a given SR pair among source regions at northern mid-latitudes [TF HTAP, 2007
168 and references therein]. Comparison among prior studies, however, is limited by
169 methodological differences, including definitions of source and receptor regions, reported
170 metrics, time period of analysis, and SR calculation method [TF HTAP, 2007].
171 Observational analyses have compared concentration differences in air masses
172 originating from a source region versus a background value [e.g. Huntrieser et al., 2005;
173 Derwent et al., 1998; Jaffe et al., 2003b]. A suite of methods for source attribution have
174 | been applied in models, including marking tracers by region of O₃ production [e.g. Jaeglé
175 et al., 2003; Derwent et al., 2004], labeling by the regional NO_x source contributing to O₃
176 production [Hess and Lamarque, 2007], and sensitivity simulations in which regional
177 emissions are perturbed [e.g. Jacob et al., 1999; Yienger et al., 2000; Wild and Akimoto,
178 2001; Fiore et al., 2002b, Auvray and Bey, 2005].

179 The approach adopted here builds upon these previous studies by applying a
180 consistent experimental design across multiple models to provide an estimate of SR
181 relationships throughout the year. Specifically, we investigate the changes in surface O₃
182 resulting from fixed percentage reductions in anthropogenic O₃ precursors (NO_x, CO,
183 CH₄, and NMVOC). We first describe the modeling framework (Section 2) and evaluate
184 the base case simulations with observations of surface O₃ (Section 3). Our analysis

185 focuses on two SR metrics: (1) the response, defined as the spatially averaged absolute
186 change in O₃ concentrations over a receptor region due to emission changes in the source
187 region, and (2) the “import sensitivity”, defined as the ratio of the sum of the changes in
188 surface O₃ resulting from perturbations to precursor emissions in the three foreign source
189 regions to the surface O₃ change resulting from the same percentage perturbation to
190 domestic emissions (*i.e.*, emissions within the continental receptor region; Section 4).
191 We then examine the response of surface O₃ to changes in CH₄ levels (Section 5). In an
192 effort to relate our results more directly to statistics commonly employed in air quality
193 management, we also analyze the response of a threshold indicator of air quality to
194 emission changes (Section 6). Finally, we assess the consistency of observed trends in
195 surface O₃ in recent decades to those derived by applying our SR relationships to
196 estimated trends in regional precursor emissions (Section 7).

197

198 **2. Model Simulations and Emissions**

199

200 The 21 chemical transport models (CTMs) that conducted simulations designed to
201 estimate source-receptor (SR) relationships for O₃ are described in Table A1 (auxiliary
202 material). Initial results were reported by *TF HTAP* [2007]; we expand here upon that
203 analysis. All modeling groups used meteorology from the year 2001 and horizontal
204 resolution of 5°x5° or finer. Most models were driven by meteorological fields from one
205 of several reanalysis centers (either prescribed directly or via linear relaxation) although 2
206 models were general circulation models with meteorology generated based on observed
207 sea surface temperatures for 2001 (Table A1). About half of the models had resolutions
208 of 3°x3° or finer, similar to the ACCENT/AR4 intercomparison [Dentener *et al.*, 2006;
209 Stevenson *et al.*, 2006]. CH₄ concentrations were set to a uniform mixing ratio of 1760
210 ppb and modeling groups were requested to use their best estimate for emissions of O₃
211 precursors (Tables A2 and A3), so the results include uncertainties associated with the
212 use of different emission inventories.

213

214 We consider four major source regions at northern mid-latitudes (Figure 1): East
215 Asia (EA), Europe and northern Africa (EU), North America (NA), and South Asia (SA).
216 The EU and EA regions span roughly equivalent areas (2.1x10⁷ and 2.3x10⁷ km²), with
217 NA somewhat larger (2.6x10⁷ km²) and nearly twice the area of SA (1.5x10⁷ km²).
218 According to the model ensemble mean (μ), similar quantities of anthropogenic NO_x and
219 NMVOC are emitted from EU, NA, and EA (to within ~30%; Table 1; see Tables A2 and
220 A3 for the emissions used by individual models). The standard deviation (σ) indicates the
221 diversity of the emission inventories used in the models, with the smallest inter-model
222 spread for anthropogenic NO_x emissions in EU and NA ($\sigma/\mu < 10\%$) and the largest
223 spread for anthropogenic VOC from EU ($\sigma/\mu = 58\%$). A comparison of the model
224 ensemble mean anthropogenic and total (which also includes biomass burning and
225 biogenic contributions) emissions in Table 1 shows a dominant contribution (>70%) from
226 anthropogenic NO_x and CO in all regions considered. For the ensemble mean NMVOC
227 emissions, biogenic emissions dominate in all regions except for EU where
228 anthropogenic and biogenic contributions are approximately equal.

229

230 In the base simulation (SR1), the 21-model annual spatial mean surface O₃ mixing
ratios and their standard deviations over the four continental source regions in Figure 1
are similar: 36.2±3.9 ppb for NA, 37.8±4.5 for EU, 35.8±3.0 for EA, and 39.6±4.0 for

231 SA. The largest ensemble mean seasonal amplitude (difference between the maximum
232 and minimum months) occurs in EU (19.8 ± 5.9 ppb), possibly reflecting NO_x titration in
233 the stronger wintertime boundary layer compared to the other regions (10.4 ± 2.6 for NA;
234 12.7 ± 3.2 for EA, and 14.8 ± 6.0 for SA).

235 Relative to SR1, we conduct 16 sensitivity simulations in which anthropogenic
236 emissions of the traditional O_3 precursors (NO_x , NMVOC, and CO) are reduced by 20%
237 individually (simulations SR3, SR4, and SR5, respectively) and jointly along with
238 aerosols (“ALL”; simulation SR6) within each of the four source regions in Figure 1.
239 These simulations are labeled hereafter according to the respective emission scenario and
240 the region in which emission reductions were applied (*e.g.*, SR3EA identifies the
241 simulations with 20% reductions of anthropogenic NO_x emissions within East Asia). An
242 additional sensitivity simulation was conducted in which the CH_4 mixing ratio was
243 decreased by 20% (to 1408 ppb) and other O_3 precursor emissions were held constant
244 (SR2). All simulations were conducted for a full year, following a minimum of six
245 months initialization, a sufficient time for the simulated trace gas concentrations to fully
246 respond to the imposed emission or concentration perturbations given our use of uniform
247 CH_4 mixing ratios; responses on longer time scales are diagnosed in Section 5.

248 The perturbation magnitude of 20% was chosen for two reasons: (1) A reduction
249 of this magnitude is expected to be feasible on a decadal time frame and is thereby
250 relevant to air pollution policy, and (2) it reflects a compromise between producing a
251 clear signal in the O_3 simulations and applying a sufficiently small perturbation to allow
252 the results to be scaled linearly to different size perturbations. Under the ACCENT/AR4
253 Experiment 2, *Stevenson et al.* [2006] found a broadly linear relationship between the 26-
254 model mean tropospheric O_3 burden and global NO_x emissions within the $\pm 50\%$ range of
255 present day emissions considered in that study, although those simulations did not
256 exclusively change NO_x emissions. The scalability of our results to perturbations of other
257 magnitudes is examined further for NO_x in Section 4.2, and has been shown to hold for
258 the O_3 response to changes in CH_4 over the range of present-day anthropogenic emissions
259 [*Fiore et al.*, 2008]. We further assume that the O_3 responses to regional perturbations can
260 be summed to approximate the O_3 response to simultaneous reductions in multiple
261 regions.

262

263 | 3. Model Evaluation with Surface Observations

264

265 A major challenge to assessing model skill at representing intercontinental SR
266 relationships arises from the difficulty of directly observing these relationships
267 (particularly in surface air). Testing the models with simultaneous measurements of O_3
268 and related species is preferable [*e.g.* *Sillman*, 1999]; such observations are mainly
269 limited to intensive field campaigns, which are the focus of an ongoing TF HTAP multi-
270 model study. A companion study will evaluate the models with the ozonesonde network
271 [*Jonson et al.*, in prep]. Many of the models in our study have been compared with ozone
272 observations for the year 2000 as part of the ACCENT/AR4 Experiment 2 study [*e.g.*,
273 *Dentener et al.*, 2006; *Stevenson et al.*, 2006; *Ellingsen et al.*, 2008]. Comparison with
274 observations from the global ozonesonde network [*Logan*, 1999] across different latitude
275 and altitude bands showed that the overall multi-model root mean square error (RMSE)
276 was 5.9 ppb, ranging from 5.1 to 18 ppb across the models [*Stevenson et al.*, 2006].

277 Annual mean surface O₃ concentrations were within 5 ppb of the measurements in the
278 United States, China, and Central Europe [Dentener *et al.*, 2006]. Overestimates of 10-
279 15 ppb were found in Africa, India, and the Mediterranean, for reasons not yet
280 understood [Dentener *et al.*, 2006; Ellingsen *et al.*, 2008].

281 Due to limited availability of surface O₃ measurements over India, China, and
282 Africa, we focus here on the widespread observational networks in the United States,
283 Europe, and Japan (Figure 2). While the individual models often differ by more than 15
284 ppb, the model ensemble mean generally captures the observed seasonal cycle and is
285 close to the observed regional mean. A wide range of simulated tropospheric O₃ budgets
286 has been documented in the literature, attributed in part to factors that are likely to
287 contribute to inter-model variability in simulated surface O₃ concentrations, such as
288 differences in surface emissions of NO_x and isoprene, as well as in model treatment of
289 dry deposition, heterogeneous chemistry and the organic nitrates from isoprene
290 [Stevenson *et al.*, 2006; Wu *et al.*, 2006; Wild, 2007; Ellingsen *et al.*, 2008].

291 We separate the observational sites at low elevations from those at higher
292 altitudes since high altitude sites more frequently sample free tropospheric air and thus
293 are better suited to detecting hemispheric pollutant transport (which occurs most
294 efficiently in the free troposphere) prior to mixing with local pollutant signals in the
295 planetary boundary layer [Cooper and Moody, 2000; Trickl *et al.*, 2003; Weiss-Penzias *et*
296 *al.*, 2006]. At the high altitude sites (Figures 2c and 2h), the models tend to
297 underestimate O₃ concentrations. Steep topographic gradients that are averaged out
298 within one model grid cell, particularly over Europe, may be responsible if the
299 measurements are more representative of the free troposphere than the models' surface
300 layer (where O₃ deposition leads to lower concentrations). During the cold season, the
301 underestimate could also reflect insufficient transport from the stratosphere [Shindell *et*
302 *al.*, 2006].

303 The model ensemble mean and median exhibit little bias at low-altitude European
304 sites and capture the seasonal cycle (Figures 2a and 2b), an apparent improvement over
305 the underestimate in summer months found by Ellingsen *et al.* [2008]. In contrast, the
306 multi-model mean overestimates the observed summertime surface O₃ concentrations
307 over Japan (bias of 12 ppb; Figure 2i) and in the eastern U.S. (bias greater than 15 ppb in
308 July in Figures 2d, 2f and 2g). The observed summer minimum in O₃ over Japan occurs
309 during the wet season of the Asian monsoon. Results from the MICS-Asia regional
310 model intercomparison suggest that the positive model bias may stem from inadequate
311 representation of southwesterly inflow of clean marine air [Han *et al.*, 2008; Holloway *et*
312 *al.*, 2008]. Examination of inter-model differences in this region with the TF HTAP
313 idealized tracer transport simulations [Schultz *et al.*, in prep] should provide further
314 insights into the source of this problem.

315 Ellingsen *et al.* [2008] also found an overestimate of surface O₃ levels in July
316 through September for the year 2000 over the Great Lakes, and in June through
317 September over the Southeastern United States. In July and August, however, the
318 ensemble median value fell within the standard deviation of the observations. We find
319 that the observed July and August average O₃ decreased by 10 ppb from 2000 to 2001;
320 the larger model error shown in Figure 2 than found by Ellingsen *et al.* [2008] suggests
321 that the model ensemble mean does not capture the observed interannual variability over
322 the eastern United States, although our use of different emission inventories from

323 *Ellingsen et al.* [2008] may also play a role. The bias is particularly large over the
324 southeastern U.S. where uncertainties in isoprene-NO_x-O₃ chemistry may contribute;
325 smaller biogenic NMVOC emissions over Europe (difference between total and
326 anthropogenic NMVOC in Table 1) would lessen the impact of any problems in this
327 chemistry on surface O₃ concentrations there. The bias is not driven by nighttime
328 processes since restricting our comparison to afternoon hours does not yield any
329 improvement (Figure A1). The models do not account for the observed decrease in U.S.
330 power plant NO_x emission reductions that occurred between 1999 and 2003 (~50%
331 decrease averaged over 53 power plants) [*Frost et al.*, 2006]. Comparison with the
332 SR3NA simulations (in which North American anthropogenic NO_x emissions are
333 decreased by 20%, roughly the total emission reduction contributed by the power plants),
334 however, decreases the bias by only 2-4 ppb. The occurrence of the eastern U.S. bias in
335 summer strongly suggests an overestimate of regionally produced O₃. The sensitivity of
336 surface O₃ over all regions to foreign sources is strongest in spring and late autumn
337 (Section 4), however, when the model ensemble mean matches the observed values in all
338 regions, lending confidence to our results for those seasons.

339

340 **4. Source-Receptor Relationships for NO_x, NMVOC and CO**

341

342 *4.1 Model Ensemble Mean Results*

343 Figure 3 (and Table A4) shows the annual average surface O₃ response in the
344 receptor regions to 20% regional reductions of anthropogenic NO_x, CO, NMVOC
345 emissions, individually and all together (“ALL”), as well as the sum of the responses to
346 emission perturbations in the “3 foreign” source regions. In most receptor regions, O₃
347 responds most strongly to NO_x, followed by NMVOC and CO, respectively. An
348 exception occurs for EU emissions where the model ensemble O₃ response to NMVOC,
349 for foreign SR pairs, is comparable to that from NO_x. The relative dominance of NO_x
350 diminishes when the long-term feedback through CH₄ is taken into account (Section 5).
351 For all SR pairs, domestic emission reductions are most effective at reducing surface O₃.
352 Surface O₃ also decreases when emissions are reduced in a foreign source region, often
353 by more than 10% of the decrease attained with the same percentage emission reduction
354 applied domestically (Figure 3 and bold entries in Table A4). The largest annual mean
355 responses to foreign emissions are ~50% of the response to domestic emissions and occur
356 for NA NO_x, CO, and ALL on EU surface O₃, and for EU NMVOC on SA surface O₃.

357 We next examine seasonality in these SR relationships, beginning with the
358 seasonal cycle in the O₃ response to domestic emission reductions (filled circles in Figure
359 4). Over all regions, the domestic response to the 20% decrease in CO emissions (~0.1
360 ppb) varies little during the year while the response to NO_x exhibits the strongest
361 seasonality (max of >1 ppb). Over EU, NO_x reductions increase the model ensemble
362 mean O₃ from November to March. The response to NMVOC emission reductions is
363 largest in boreal winter (up to ~0.5 ppb over EU, though seasonality is weak), when
364 biogenic emissions, radiation, and humidity are at their seasonal minimum and O₃
365 production is more sensitive to anthropogenic NMVOC [*Jacob et al.*, 1995]. The
366 seasonality of the domestic response to ALL is largely driven by NO_x, peaking in
367 summer for NA, EU, and EA, and in October through March for SA. The different

368 seasonality over SA reflects the influence of the Asian monsoon (wet season during
369 summer).

370 We find a larger contribution of intercontinental transport at northern mid-
371 latitudes to surface O₃ concentrations during boreal spring and fall (filled circles in
372 Figure 5), reflecting a combination of more frequent storm tracks that enhance ventilation
373 of the continental boundary layer, more efficient transport in stronger mid-latitude
374 westerly flow in the free troposphere, and a longer O₃ lifetime allowing for a longer
375 transport distance than in summer when O₃ chemical production and loss are largest
376 [Wang *et al.*, 1998; Jaffe *et al.*, 1999; Yienger *et al.*, 2000; Bey *et al.*, 2001; Wild and
377 Akimoto, 2001; Liu *et al.*, 2003; Stohl *et al.*, 2002; Weiss-Penzias *et al.*, 2004; Wild *et al.*,
378 2004; Holzer *et al.*, 2005; Holloway *et al.*, 2008]. Over all regions, the response to 20%
379 decreases in anthropogenic NO_x emissions from all 3 foreign regions combined are
380 largest in boreal spring and fall to early winter (up to ~0.4 ppb); the response to foreign
381 NMVOC emissions is largest in winter through early spring (0.2-0.4 ppb). Over NA, the
382 model ensemble average O₃ response to foreign NO_x and NMVOC are similar (~0.3 ppb)
383 in winter, spring and summer, although this result varies across models (Section 4.3).
384 The 20% reductions in foreign emissions of CO have little influence (<0.2 ppb) on
385 surface O₃ over the receptor regions, but this influence increases when the long-term
386 feedback via CH₄ is included (Section 5.2).

387 In Figure 6, we show the surface O₃ response in each receptor region to ALL, and
388 decompose the total foreign impact into the contributions from each of the three foreign
389 source regions. For the NA receptor region, EA and EU contribute similarly from April
390 through November. NA contributes most strongly to EU throughout the year, reflecting
391 its relative upwind proximity. The SA source region exerts a minor influence throughout
392 the year over NA and EU (always less than 0.1 ppb to surface O₃), as SA pollution is
393 typically funneled away from the northern mid-latitude westerlies (the dominant transport
394 pathway to those regions) [*e.g.*, Li *et al.*, 2001; Lelieveld *et al.*, 2002a; TF HTAP 2007],
395 and tends to remain isolated from mid-latitude air [Bowman and Carrie, 2002; Hess,
396 2005]. Over EA, emissions from the three foreign source regions induce a similar
397 response in surface O₃ during summer, with stronger sensitivity to emissions in EU
398 (followed by NA) during spring, and to NA (followed by EU) in winter. Over SA, the
399 surface O₃ response is largest when emissions are reduced in EU, except for the
400 November peak which is driven by emissions from EA. We conclude that EU is
401 influenced most strongly by NA throughout the year, but that the other receptor regions
402 exhibit similar responses to emission reductions in at least two of the foreign source
403 regions.

404 In order to compare the surface O₃ response to foreign versus domestic emissions,
405 we define an “import sensitivity” (IS_r):

406
$$IS_r = \left(\sum_{f=1}^3 \Delta O_{3fr} \right) / \Delta O_{3tr}$$

407 where IS_r represents the import sensitivity for receptor region r; ΔO_{3fr} represents the
408 model ensemble mean change in surface O₃, spatially averaged over the receptor region r,
409 produced by a 20% decrease in anthropogenic emissions over the foreign source region
410 (f); ΔO_{3tr} is the change in surface O₃ resulting from the 20% reduction of anthropogenic
411 emissions within the domestic source region. The larger the value of the import
412 sensitivity, the greater the influence of foreign emissions. The annual mean IS_r ranges

413 from approximately 0.3 (NA and SA) to 0.75 (EU) for NO_x alone; 0.4 (EU) to 1.1 (SA)
414 for NMVOC alone; and 0.45 (NA and SA) to 0.75 (EU) for the combined reductions in
415 all O₃ precursors. The IS_r is typically largest for CO, ranging from approximately 0.9
416 (EA) to 1.1 (EU), reflecting the longer CO lifetime and the correspondingly smaller
417 influence from domestic sources.

418 Monthly mean IS_r estimates from the ALL simulations are shown in Figure 7.
419 Over EA, NA, and EU, the IS_r exceed one during boreal winter (also in spring and fall
420 over EU) when O₃ production from domestic emissions is small (Figure 4). Even in
421 summer, when domestic O₃ production peaks, IS_r is 0.2-0.3 over these regions. During
422 the month with the largest surface O₃ response to ALL foreign emission reductions
423 (Figures 5 and 6), IS_{NA}=0.6 (April), IS_{EU}=0.7 (April), and IS_{EA}=1.1 (March). The IS_{SA}
424 for ALL varies little during the year and is ~0.5 in November and during the broad
425 secondary peak from January through April (Figures 6 and 7). We conclude that the O₃
426 response to foreign emissions is not negligible when compared to the response to
427 domestic emissions, and is particularly strong in spring and fall at northern mid-latitudes.
428

429 *4.2 Applicability of Results to Other Emission Perturbations*

430 Evaluating whether the O₃ response to multi-component emission reductions is
431 equivalent to the sum of the responses to single component emission reductions is critical
432 for determining the applicability of our results to other combinations of precursor
433 emission reductions. In order to assess the additivity of our simulations, we construct the
434 ratio of the sum of the O₃ response to 20% reductions in emissions of the individual
435 precursors (SR3-SR1)+(SR4-SR1)+(SR5-SR1) to the O₃ response in the simulation
436 where all precursors (along with aerosols) were reduced simultaneously (SR6-SR1). With
437 one exception, models including reductions of aerosols and precursors in SR6 indicate
438 that the sum of the responses to single component emission reductions exceeds that to
439 multi-component perturbations, by as much as 50% for some SR pairs (Table A5 and
440 Figure A3). Ranking all of the models by the NA domestic response shows that the
441 degree of additivity varies by region within individual models (Figure A3). In Figure 8,
442 we restrict our analysis to those models without aerosol changes in SR6, and find that the
443 responses to single-component versus multi-component emission reductions are
444 approximately equivalent for the O₃ responses to domestic and foreign emissions. We
445 conclude that combined reductions in emissions of aerosols and O₃ precursors dampen
446 the O₃ response relative to that produced by emission reductions of the O₃ precursors
447 alone.

448 If we wish to apply the responses diagnosed in Section 4.1 more broadly, we need
449 to determine if the O₃ response is sufficiently linear to yield accurate results when scaling
450 to emission perturbations of other magnitudes. To address this point, additional
451 simulations with varying sizes of perturbations to EU anthropogenic NO_x emissions were
452 conducted in the FRSGC/UCI model [Wild *et al.*, 2003]. The FRSGC/UCI model tends
453 to produce a larger surface O₃ response to NO_x than the model ensemble mean, but is not
454 an outlier in any month, so we expect these results to apply generally to our model
455 ensemble. Figure 9 shows the response of surface O₃ over EU and NA. The EU source
456 region was chosen as it exhibits the most non-linear response of all regions (*e.g.*,
457 reversing sign with season in Figure 4). The response over the source region (EU)
458 deviates more from that obtained by a linear scaling of the response in the 20%

459 perturbation simulation than over a remote receptor region (NA). For example, the
460 summertime response over the EU remains linear only for perturbations within 20%,
461 whereas it is linear well beyond perturbations of 50% over NA. The scalability of the
462 results shows that the response is most linear in summer over the foreign receptor region.
463 A companion manuscript [Wu *et al.*, in preparation] will explore the processes
464 contributing to the seasonal dependence in Figure 9, incorporating simulations from other
465 models, perturbations to other O₃ precursor emissions and emissions from other source
466 regions.

467 4.3 Robustness of Results as Measured by Inter-model Differences

468 It is notoriously difficult to attribute uncertainty to model results. The range
469 spanned by the SR relationships among the models provides a measure of uncertainty as
470 encompassed by differences in the emission inventories and the representations of
471 transport and photochemical processes in the individual models. The uncertainty
472 (measured by the standard deviation divided by the mean (*i.e.*, σ/μ)) associated with the
473 O₃ response to decreases in NMVOC emissions is often larger than that due to reductions
474 in either NO_x or CO emissions (Table A4), and probably reflects the larger uncertainty
475 associated with the NMVOC inventories and the incorporation of the individual NMVOC
476 species into the model chemical mechanisms (Table 1).

477 Figure 5 suggests that surface O₃ over NA has a similar sensitivity to foreign
478 emissions of NO_x and NMVOC, but this result varies across the individual models (not
479 shown). For example, Figure 10 shows that the magnitude of the surface O₃ response
480 over NA to decreases in EU anthropogenic NMVOC emissions in the individual models
481 correlates ($r^2 = 0.50$) with the anthropogenic EU NMVOC emission total, which varies by
482 nearly a factor of 10. Better constraints on the total NMVOC emissions and their
483 partitioning into NMVOC species with different reactivity should help to reduce the
484 associated uncertainty in the O₃ sensitivity. While the model ensemble mean response in
485 Figure 5 is most sensitive to NO_x, this result only holds for all individual models over
486 SA. We recommend a future study to probe more deeply into the sources of model
487 differences in the surface O₃ sensitivity to NO_x versus NMVOC.

488 We examine whether the bias in the individual models over the eastern United
489 States (Section 3) manifests as a larger response, for example, of EU surface O₃ to the
490 reductions in NA emissions. We find little correlation with the simulated SR relationships
491 ($r^2 < 0.1$ for the EU response to NA emission changes in July). The source of the bias,
492 however, should be understood to increase confidence in the estimates for summertime
493 SR relationships for the NA and EA regions.

494 For each region, we further assess the robustness of the SR relationships in Figure
495 6 across the 15 individual models. We focus here on the springtime (March, April and
496 May) and annual average response to the combined emissions reductions (*i.e.*, SR6-SR1).
497 The rankings for the EU receptor region are most robust, with NA>EA>SA in all models
498 except for one where the annual mean response to emissions in EA and SA are equal. All
499 models also indicate that annual and springtime mean O₃ over EA, EU, and NA is less
500 sensitive to emissions from SA versus the other three foreign regions. The model spread
501 in the response of NA surface O₃ to emission reductions in EU versus EA in spring
502 indicates more uncertainty, with 10 models predicting equivalent responses (to within
503 20%), but in 4 models the response to EA emissions is 30-55% greater than that to EU
504

505 emissions. For the annual mean NA O₃ response, 8 models predict equivalent responses
506 while 6 suggest that the response to EA emissions is 25-50% larger than that to EU
507 emissions. Over EA, where the winds are northwesterly during spring, the O₃ response to
508 emission changes in EU and NA exceeds that to SA (by a factor of 1.6-3 for EU in 12
509 models, and 1.5-2 for NA in 9 models); even in the annual mean results, 12 models
510 simulate a larger response to emissions from EU and/or NA than from SA. Over SA, the
511 O₃ response to emission changes rank as EU>NA>EA in 9 of 15 models for spring (but
512 this ranking holds for only 3 models in the annual mean, with 9 models predicting annual
513 mean responses within 20% in at least two of the source regions).

514 The rankings of individual models often change with season, likely reflecting
515 seasonal variations in transport pathways. Year-to-year fluctuations in transport
516 pathways may also alter the rankings of the foreign source influence. For example, the
517 NA influence on EU surface O₃ in late winter and early spring in years with a positive
518 Arctic Oscillation (AO) index is likely larger than that estimated for 2001 (negative AO)
519 since a positive AO index is associated with warm conveyor belts positioned to transport
520 pollution more efficiently from the northeastern United States to EU [Eckhardt *et al.*,
521 2004; Lamarque and Hess, 2004; Hess and Lamarque, 2007]. The influence of EU
522 emissions on NA surface O₃ is also expected to be stronger in years with a positive AO
523 index [Hess and Lamarque, 2007]. With respect to indices for trans-Pacific transport, the
524 year 2001 should be representative of an average year [Liang *et al.*, 2005; Liu *et al.*,
525 2005]. The robustness of the rankings identified here to interannual variability deserves
526 further study.

527

528 *4.4 Comparison with prior estimates of intercontinental source-receptor relationships*

529 In Figure 11, we compare our results for the NA, EU, and EA regions with the
530 studies referenced in the TF HTAP [2007] that report annual and seasonal mean SR
531 relationships, supplemented by recent analyses by Lin *et al.* [2008], Duncan *et al.* [2008],
532 and Holloway *et al.* [2008]. While the range across previous studies reflects a variety of
533 regional definitions, reported metrics, meteorological years, and methods for source
534 attribution, the consistent modeling approach adopted here restricts the uncertainty as
535 represented by the range across our model results to differences in emissions, chemistry,
536 and transport. Information regarding import to or export from the SA region is limited;
537 our results in Figure 5 for SA are consistent with those of Kuhnkrishnan *et al.* [2006] in
538 showing an autumn peak, but in contrast to that study, we find that the response of SA
539 surface O₃ to EA NO_x emissions is larger in winter than in summer.

540 In cases where an emission perturbation was not a 100% decrease, we scale the
541 reported O₃ response to estimate the total contribution from the foreign emissions. For
542 example, we use 5*(SR1-SR6) to estimate the total contribution of anthropogenic
543 emissions of the traditional O₃ precursors (NO_x+NMVOC+CO) from a foreign source to
544 a receptor region. Figure 10 implies that a linear scaling of our 20% reductions in
545 anthropogenic NO_x emissions will yield a smaller response than that in a simulation
546 where emissions are set to zero. We expect the response to the combined
547 NO_x+NMVOC+CO emission reductions to deviate less from linearity due to the
548 competing effects on OH from NO_x versus NMVOC+CO but this assumption needs
549 further investigation. The range in annual mean SR relationships for the EU and EA
550 receptor regions across our model ensemble narrows considerably from the estimates in

551 the literature, with the model ensemble response in Figure 11 smaller than most prior
552 estimates for spring and summer. Our study provides a comprehensive view of the
553 seasonality of SR relationships and a previously unavailable quantitative measure of
554 uncertainty in these relationships.

555

556 **5. Contribution from CH₄ to the long term response of O₃**

557

558 *5.1 Surface O₃ response to CH₄ concentrations*

559 The annual mean surface O₃ response to a 20% decrease in global CH₄
560 concentrations is 1.1-1.3 ppb over the receptor regions, largest in SA and EU, followed
561 by NA and EA (Table A4). The O₃ responses in the individual models, however, differ
562 by ~1 ppb. This uncertainty is likely to stem from model differences in OH and NO_x
563 distributions [e.g., Fiore *et al.*, 2008]. As the O₃ response to CH₄ is approximately linear
564 over the range of present-day anthropogenic emissions [Fiore *et al.*, 2008], scaling the
565 ensemble mean responses in Table A4 from 20% to 100% implies that CH₄ presently
566 contributes 5.5-6.5 ppb of the surface O₃ in the receptor regions.

567 The tropical location of SA leads to the stronger O₃ response to CH₄ since CH₄
568 oxidation predominantly occurs in the tropical lower troposphere due to the combination
569 of OH availability and the temperature sensitivity of the CH₄-OH rate constant [e.g.,
570 Spivakovsky *et al.*, 2000]. One might expect that EU, situated at more northerly latitudes
571 than the other regions, would exhibit the weakest response of surface O₃ to CH₄. Instead,
572 the response is nearly as strong as that found in SA, and stronger than the responses in
573 NA and EA. The largest seasonal amplitude of the O₃ response to CH₄ (difference
574 between the maximum and minimum monthly mean values) occurs in EU, followed by
575 SA, NA, and EA (Figure A4). The O₃ response to CH₄ over EU is largest during
576 summer, possibly reflecting a combination of the stronger seasonality in O₃ production in
577 this northernmost region and stronger CH₄-sensitivity arising from smaller biogenic (high
578 reactivity) VOC emissions than in the other regions. The seasonal amplitude of the EU
579 O₃ response to CH₄ in the individual models is indeed somewhat correlated with the ratio
580 of EU anthropogenic to total NMVOC emissions ($r = 0.6$ for 13 models).

581

582 *5.2 Long-term O₃ response to NO_x, CO, NMVOC emissions reductions*

583 Perturbations to NO_x, NMVOC and CO emissions influence the oxidizing
584 capacity of the atmosphere (OH), which can change the CH₄ lifetime and thereby
585 contribute a “long-term” change in tropospheric O₃ on the decadal time scale of the CH₄
586 perturbation lifetime [e.g. Prather, 1996; Daniel and Solomon, 1998; Fuglestvedt *et al.*,
587 1999; Wild and Prather, 2000; Derwent *et al.*, 2001; Wild *et al.*, 2001; Collins *et al.*,
588 2002; Stevenson *et al.*, 2004]. West *et al.* [2007] previously found that the long-term
589 impacts of 20% decreases in global anthropogenic emissions on population-weighted
590 average surface O₃ at northern mid-latitudes enhanced the short-term response by 16-
591 21% for CO, and decreased it by 6-14% for NO_x, with little long-term influence from
592 NMVOC. This long-term impact on surface O₃ exhibits the spatial distribution of the
593 surface O₃ response to changes in CH₄, which we obtain from the difference in O₃
594 between the SR2 and SR1 simulations (Section 5.1). By setting atmospheric CH₄ to a
595 uniform, fixed value of 1760 ppb, the SR3 through SR6 simulations neglect the feedback
596 on CH₄ from the changes in OH induced by the 20% decreases in regional anthropogenic

597 NO_x, NMVOC, and CO emissions. In order to account for this feedback, we first
 598 estimate what the CH₄ concentration change would be in a simulation with the same CH₄
 599 loss by OH as in the perturbation simulation, but with CH₄ emissions held equal to those
 600 implied by the 1760 ppb atmospheric abundance in SR1.

601 We apply the formulation of *West et al.* [2007] to estimate the CH₄ abundance that
 602 would result from the changes in the other O₃ precursor emissions:

603

$$604 \quad [\text{CH}_4]_{\text{SRNxx}} = [\text{CH}_4]_{\text{SR1}} * (\tau_{\text{SRNxx}} / \tau_{\text{SR1}})^F$$

605

606 where SRN represents SR3 through SR6; xx is the 2-letter regional abbreviation in Figure
 607 | 1; τ_{SR1} is the total atmospheric CH₄ lifetime in the base simulation; τ_{SRNxx} is the CH₄
 608 lifetime in the perturbation simulation; and F is defined as the ratio of the atmospheric
 609 response (perturbation) time to the global atmospheric lifetime (see below). Table 2 lists
 610 the subset of models that archived the CH₄ loss rates required to determine τ_{SR1} , τ_{SRNxx} ,
 611 and F. The model ensemble mean $\tau_{\text{SR1}} = 8.55 \pm 1.6$ is within 2% of the 26-model mean
 612 of 8.67 ± 1.32 reported by *Stevenson et al.* [2006]. From the SR1 and SR2 simulations,
 613 we calculate F following *Wild and Prather* [2000]:

614

$$615 \quad F = 1/(1-s)$$

616

$$s = (\ln(\tau_{\text{SR2}}) - \ln(\tau_{\text{SR1}})) / (\ln(B_{\text{SR2}}) - \ln(B_{\text{SR1}}))$$

617

618 where B is the total atmospheric CH₄ burden. F describes the response of the
 619 atmospheric CH₄ abundance to a change in CH₄ emissions. In the case of a small
 620 perturbation, F is approximately the ratio of the relative change in CH₄ concentrations to
 621 an imposed emission change; for example, the model ensemble mean F of 1.33 (Table 2)
 622 implies that a 1% increase in CH₄ emissions would ultimately yield a 1.33% increase in
 623 CH₄ concentrations. The multi-model mean F is at the low end of the 1.33 to 1.45 range
 624 reported (and within 10% of the recommended F of 1.4) by *Prather et al.* [2001].

625 Following *Naik et al.* [2005] and *West et al.* [2007], we estimate the long-term
 626 impact on O₃ by scaling the change in surface O₃ in the CH₄ perturbation simulation
 627 (SR2-SR1) by the ratio of the estimated changes in CH₄ from SR1 to SRNxx versus SR2:

628

$$629 \quad \Delta\text{O}_3 (\text{SRNxx} - \text{SR1}) = [\Delta\text{CH}_4 (\text{SRNxx} - \text{SR1}) / \Delta\text{CH}_4 (\text{SR2-SR1})] * \Delta\text{O}_3 (\text{SR2-SR1})$$

630

631 For each model, we add this ΔO_3 to the short-term O₃ response diagnosed directly from
 632 SRNxx-SR1.

633

634 Including the long-term feedback through CH₄ has little impact on the model
 635 ensemble mean domestic response (solid vs. dotted lines in Figure 4). In contrast, a
 636 larger percentage change occurs for the O₃ response to foreign emissions since the O₃
 637 response to changes in CH₄ (SR2-SR1) is relatively uniform globally. Figure 5 shows
 638 that the long-term contribution diminishes the estimated O₃ response to foreign NO_x
 639 emissions by ~15-20% during the month of maximum foreign contribution (April for
 640 NA, EU, and EA and November for SA) since decreasing NO_x lowers OH, causing the
 641 CH₄ abundance to rise, thereby enhancing the CH₄ contribution to surface O₃. During the
 642 same months, the short-term O₃ responses to the 20% reductions in foreign CO and
 NMVOC emissions are augmented by 30-40% and ~10%, respectively, since decreasing

643 CO or NMVOC increases OH. These results are qualitatively consistent with those of
644 *West et al.* [2007]. Over NA and EU during summer, the opposing influences of the
645 long-term feedback from NO_x and CO result in the total impact of the CO emission
646 reductions exceeding that from NO_x (or NMVOC). As there is little seasonality in the O₃
647 response to CH₄ (SR2-SR1), the seasonal cycle of the total O₃ response is mainly driven
648 by the short-term response to the changes in NO_x, CO, and NMVOC emissions (Figure
649 6).

650 In the case of “ALL”, the long-term feedback is minimal (always less than 3% for
651 all months and regions in Figure 5). The balancing effect of simultaneous changes of
652 NO_x, CO, and NMVOC has been noted before in the context of the remarkable stability
653 | of OH concentrations from the pre-industrial to the present-day atmosphere [*Wang and*
654 *Jacob*, 1998; *Lelieveld et al.*, 2002b]. Since anthropogenic sources of NO_x, CO, and
655 NMVOC differ, however, equivalent percentage reductions would not necessarily be
656 applied to all precursors together, in which case the long-term effect should be
657 considered.

658

659 | 5.3 Inferring the O₃ response to regional reductions in anthropogenic CH₄ emissions

660

661 Since the global CH₄ abundance was decreased uniformly by 20%, the results
662 from this simulation are not directly comparable with those from the 20% regional
663 reductions of the other O₃ precursors. In this section we attempt such a comparison by
664 approximating the surface O₃ response that would result from 20% reductions of CH₄
665 anthropogenic emissions in the source regions.

666 We first use ensemble mean results to estimate the anthropogenic CH₄ emission
667 decrease that would produce the 20% reduction in global concentrations applied in the
668 SR2 simulation. Applying the model ensemble mean feedback factor (F) of 1.33 from
669 Table 2 (Section 5.1) to account for the feedback of CH₄ on its own lifetime, we derive
670 that the 20% decrease in CH₄ abundance corresponds to a 15% decrease in total global
671 | CH₄ emissions. Assuming that anthropogenic CH₄ emissions are 60% of the total CH₄
672 emissions [*Denman et al.*, 2007], this 15% decrease in total global CH₄ emissions
673 corresponds to a 25% decrease in global anthropogenic CH₄ emissions. We then use the
674 EDGAR 3.2 FT2000 anthropogenic CH₄ emission inventory [*Olivier et al.*, 2005] to
675 estimate that NA, EU, SA, and EA each contribute 16.6%, 16.0%, 17.3%, and 19.0%,
676 respectively, to total global anthropogenic emissions (298 Tg CH₄ yr⁻¹ in 2000); together
677 the anthropogenic CH₄ emissions from these four regions contribute 68.9 % to global
678 total anthropogenic emissions.

679 The fraction of the total O₃ response diagnosed from SR2-SR1 that would be
680 produced by 20% decreases in regional anthropogenic CH₄ emissions can then be
681 estimated (*i.e.*, for NA: (0.2*16.6% of global anthropogenic emissions)/(25% decrease in
682 global anthropogenic emissions as implied by the concentration change in SR2),
683 assuming that the O₃ response scales linearly with changes in anthropogenic CH₄
684 emissions and does not depend on the location of the CH₄ emission reductions [*Fiore et*
685 *al.*, 2008]. We obtain values of 13.3%, 12.8%, 13.8%, and 15.2% of the O₃ decrease in
686 the SR2 simulation for NA, EU, SA, and EA, respectively. We scale the surface O₃
687 response to CH₄ over the receptor regions (SR2-SR1 in Table 2) by these values to

688 estimate an annual mean surface O₃ decrease for each SR pair (Table A6) that ranges
689 from 0.14 ppb (NA and EU on EA) to 0.20 ppb (EA on SA).

690 The results are shown in Figure 3 for comparison with the O₃ decreases achieved
691 with reductions in the regional emissions of the traditional O₃ precursors (NO_x, NMVOC,
692 and CO). While the combined domestic emission reductions of the traditional O₃
693 precursors (“ALL” in Figure 3) are most effective at reducing surface O₃ over all regions,
694 the additional inclusion of domestic CH₄ emission reductions would yield another 14-
695 20% decrease in annual mean surface O₃. Comparison of the “3 foreign” bars (black) in
696 “ALL” versus “CH₄” in Figure 3 implies that the inclusion of anthropogenic CH₄
697 emissions in a multi-species control strategy to reduce background surface O₃ in the
698 Northern Hemisphere would nearly double the surface O₃ decrease attained by
699 controlling the traditional O₃ precursors alone. The larger O₃ response over foreign
700 regions to anthropogenic CH₄ versus “ALL” O₃ precursor emissions from SA reflects the
701 comparable amounts of anthropogenic CH₄ emissions from the four regions, whereas SA
702 emits only half as much NO_x as the other regions. For 6 SR pairs, regional anthropogenic
703 CH₄ emission reductions are estimated to yield equivalent (within ±25%) responses in
704 surface O₃ over foreign continents as the coincident reductions in traditional O₃
705 precursors (ALL). For NA on EU, the influence from regional CH₄ emission reductions
706 is roughly half that of the traditional O₃ precursors, and for three SR pairs (NA on EA
707 and EU on EA and SA), the CH₄ response is 30-40% less than that to “ALL”. The
708 additional hemispheric-wide O₃ decrease from reductions in anthropogenic CH₄
709 emissions would occur on the time scale of the CH₄ lifetime, approximately a decade,
710 whereas the response to the traditional O₃ precursors will occur in weeks to months.

711

712 | **6. Response of air quality as measured by threshold statistics**

713

714 In many nations, compliance with air quality standards is assessed with respect to
715 a threshold concentration. *Ellingsen et al.* [2008] have shown that threshold statistics
716 based on 35, 60, and 80 ppb O₃, simulated by global CTMs, responded similarly to
717 changes in precursor emissions across 14 world regions ($r^2 > 0.55$). Here we focus on
718 incidences of daily maximum 8-hour average O₃ concentrations above 60 ppb
719 (DAYS>60), a statistic used in Europe to protect human health, with a target value of 25
720 | days or fewer per year [*e.g.*, as discussed further by *Ellingsen et al.*, 2008]. We
721 previously showed that the model ensemble mean closely matches the monthly average
722 O₃ observations over EU (Figure 2), and so we focus on the EMEP sites (Figure 1) to
723 compare observed and simulated DAYS>60; results are shown in Figure 12. Over the
724 Mediterranean and low-altitude (below 1 km) Central European regions several models
725 (and the model ensemble mean and median) are within the observed range of DAYS>60.
726 Consistent with the results in Figure 2, Figure 12 shows that the models tend to
727 underestimate DAYS>60 at the high-altitude central Europe with only 2 models
728 simulating values within the observed range. We recommend further work to determine
729 why some models capture this statistic better than others, including the potential role of
730 differences in mixed layer depths and deposition.

731

732 We next use the model ensemble mean values to explore the relevance of the
733 monthly mean results in Figure 6 for threshold metrics. Figure 13 shows the model
ensemble domain average monthly mean DAYS>60 in the base simulation (right axis) for

734 each region, and the change in these values when all O₃ precursors are decreased by 20%
735 in the foreign source regions (left axis). In the base simulation, DAYS>60 peaks in
736 summer over NA and EU, in spring over EA, and in winter to early spring over SA
737 (Figure 13). The response of DAYS>60 to the foreign emission reductions is strongest in
738 spring (decreases of 5-10% of the base case for some SR pairs), with the low incidence of
739 DAYS>60 in late fall preventing the secondary maximum shown in Figure 6 from
740 emerging. The rankings of the O₃ responses to foreign emission decreases in spring are
741 consistent with those in Section 4, suggesting that the mean response qualitatively
742 describes the response of the threshold statistics relevant for gauging attainment of air
743 quality standards. We emphasize that the values in Figure 13 are averaged over large
744 spatial areas and mask a large variability within the regions; for example, the model
745 ensemble mean DAYS>60 over Europe decrease by 2-4 days over much of Southern
746 Europe and Northern Africa, and by more than 5 days over the Middle East when ALL
747 emissions are decreased by 20% in NA (not shown). A forthcoming manuscript
748 [Reidmiller *et al.*] will expand this analysis further to examine variability within the
749 United States.

750 The total annual (spatial average) decrease in DAYS>60 attained with foreign
751 emission reductions is <10-20% of the decrease from equivalent percentage reductions
752 applied domestically (not shown), smaller than for the annual mean changes in Section 4.
753 This result implies that DAYS>60 (and thus higher O₃ values) are more sensitive to
754 domestic emissions, with the highest O₃ levels occurring during meteorological
755 conditions favoring regional production from domestic emissions.

756

757 **7. Consistency of O₃ trends derived from measurements versus models**

758

759 Observational evidence indicates that background surface O₃ at northern mid-
760 latitudes has been increasing by 0.1-0.5 ppb yr⁻¹ in recent decades [*e.g.* Vingarzan, 2004;
761 Carslaw, 2005; Jonson *et al.*, 2005; Derwent *et al.*, 2007; Jaffe and Ray 2007] although
762 estimated trends vary and may even be leveling off [Oltmans *et al.*, 2006; Derwent *et al.*,
763 2007]. The model ensemble mean O₃ SR relationships diagnosed here can be combined
764 with reported anthropogenic emission trends to estimate emission-driven changes in
765 Northern Hemispheric background surface O₃ for comparison with trends derived from
766 observations. While wintertime O₃ increases over Europe have been mainly attributed to
767 decreases in EU NO_x emissions [Jonson *et al.*, 2005; Ordóñez *et al.*, 2005], we consider
768 here the increase observed throughout the year, and examine the consistency of the multi-
769 model ensemble mean SR relationships with the hypothesis that a 0.1-0.5 ppb yr⁻¹
770 increase in Northern Hemispheric background O₃ may be driven by precursor emissions
771 associated with rapid industrialization in Asia [*e.g.* Jaffe *et al.* 2003c; Parrish *et al.*,
772 2004]. Recent satellite retrievals of NO₂ columns suggest that NO_x emissions from China
773 have increased by ~40%, with the growth rate accelerating from 4 to 12% per year, from
774 1996 to 2002 [Richter *et al.*, 2005]. During this same period, little change is found over
775 the United States, while the satellite NO₂ columns suggest a decrease of 30% over
776 western Europe [Richter *et al.*, 2005].

777 The annual mean surface O₃ response to EA anthropogenic NO_x emissions from
778 Table A4 (~0.1 ppb over the foreign regions) implies that a +10% yr⁻¹ increase in EA
779 NO_x emissions would yield an O₃ response of ~0.05 ppb yr⁻¹, below the observed range.

780 If we instead assume that all Asian (i.e., EA+SA) emissions are increasing together with
781 NO_x, the 20% emission reductions in Asia produce a ~0.2 (over EU) to 0.3 ppb (over
782 NA) O₃ decrease (ALL in Table A4). In this case, the 10% yr⁻¹ increase in Asian O₃
783 precursor emissions scales to an O₃ response that falls within the lower end of the surface
784 O₃ increase derived from observations: a 0.1 and 0.15 ppb yr⁻¹ increase in O₃ averaged
785 over the EU and NA receptor regions, respectively. Considering the decreases in
786 European NO_x emissions (~5% yr⁻¹), we estimate a 0.02 and 0.03 ppb yr⁻¹ annual mean
787 decrease in surface O₃ over NA and EA, respectively, or 0.04 and 0.05 ppb yr⁻¹ if EU CO
788 and NMVOC emissions follow the EU NO_x trend. We conclude that the Asian NO_x
789 emission changes estimated by *Richter et al.* [2005], if accompanied by increases in the
790 other O₃ precursors over Asia, are consistent with annual mean O₃ trends of ~0.1 ppb yr⁻¹,
791 but insufficient to produce a 0.5 ppb yr⁻¹ trend. In a similar manner, we estimate that the
792 60% increase in South Asian NO_x emissions projected by the Current Legislation (CLE)
793 emission scenario between 2005 and 2030 [*Dentener et al.*, 2005; *Cofala et al.*, 2005]
794 resulting from growth in the power and transportation sectors would increase surface O₃
795 over NA, EU, and EA by less than 0.3 ppb.

796 The ability of current models to attribute fully the observed increases in
797 background O₃ at northern mid-latitudes deserves further attention, particularly given a
798 growing demand for future projections of climate- and emission-driven changes in
799 surface O₃. Our assumptions that the NO_x trends reported by *Richter et al.* [2005] apply
800 to emissions of other O₃ precursors as well as the SA region would cause us to
801 overestimate the resulting surface O₃ trend. On the other hand, the responses diagnosed
802 here are spatially averaged over large continental regions and should be biased low
803 compared to trends derived from measurements at remote sites that are often situated on
804 the western coasts of North America and Europe, or on mountain summits where they
805 sample free tropospheric air. We expect the intercontinental signal at such sites to be
806 larger than in surface air over regions where O₃ is subjected to higher depositional and
807 chemical loss rates. In addition to rising anthropogenic emissions, regional changes in
808 climate, biogenic emissions and wildfires may contribute to the observed O₃ trends [*e.g.*,
809 *Jaffe and Ray*, 2007; *Jaffe et al.*, 2008].

810
811

812 **8. Conclusions**

813

814 Under the umbrella of the Task Force on Hemispheric Transport of Air Pollution
815 (TF HTAP; www.htap.org), we have used an ensemble modeling approach to estimate
816 source-receptor (SR) relationships for surface O₃ and its precursor emissions from four
817 continental regions at northern mid-latitudes (Figure 1). Specifically, 21 global and
818 hemispheric chemical transport models used meteorology for 2001 to simulate the impact
819 of 20% decreases in “conventional” O₃ precursor emissions (NO_x, NMVOC, and CO
820 individually and combined) from East Asia (EA), Europe (EU), North America (NA) and
821 South Asia (SA) on surface O₃ in the same four regions. Our results are intended to
822 provide a first comprehensive assessment of annual and seasonal mean intercontinental
823 SR relationships, to gauge uncertainty in these estimates, and to serve as a benchmark for
824 | future work. The consistent approach applied in our study narrows the wide range of SR
825 relationships reported in the literature (Figure 11). We identified a systematic model

826 overestimate of surface O₃ concentrations compared to observations over the eastern
827 United States and Japan, and a strong sensitivity to uncertainties in anthropogenic
828 NMVOC emissions, particularly over EU. Future work should determine the extent to
829 which our results apply to other meteorological years, and explore sub-continental
830 variability in SR relationships driven by differences in the availability of O₃ precursors
831 and in meteorological conditions [e.g., Holloway *et al.*, 2007].

832 In addition to the precursors that are traditionally regulated to abate O₃ pollution
833 (*i.e.*, NO_x, NMVOC, and CO), we examined the contribution of CH₄ to hemispheric-wide
834 surface O₃ levels, both directly by changing global CH₄ abundances, and indirectly
835 through the influence that the traditional O₃ precursors have on OH concentrations, and
836 thereby the CH₄ abundance [e.g. Prather, 1996]. Due to competing effects of CO and
837 NMVOC versus NO_x on OH, neglecting the long-term feedback when equivalent
838 percentages of CO, NMVOC and NO_x are reduced together introduces errors of at most a
839 few percent. Given the different anthropogenic sources of NO_x, CO, and NMVOC,
840 application of equivalent percentage reductions to all three precursors may not be
841 pragmatic, in which case the long-term effect may not be trivial. We further show that
842 the responses to single-component versus multi-component emission reductions are
843 approximately equivalent for the O₃ responses to changes in domestic and foreign
844 emissions, although the multi-component response is less-than-linear in coupled aerosol
845 simulations in which aerosols and their precursors were also decreased. We focus the
846 remainder of our conclusions on the simulations with the combined reductions of NO_x,
847 CO, and NMVOC.

848 For all source regions, the model ensemble mean intercontinental influence is
849 largest during spring and in late fall (Figure 6), consistent with prior studies (Figure 11
850 and Section 1). The most robust rankings across the models are that surface O₃ levels
851 over EU are influenced most strongly by emission reductions in NA, followed by EA,
852 and that SA contributes least to the three foreign regions. We find more uncertainty in
853 the relative importance of EA versus EU on NA, and of the three source regions over
854 both Asian regions. Our analysis of the impact of decreases in anthropogenic emissions
855 on the incidence of daily maximum 8-hour average O₃ concentrations above 60 ppb
856 suggests that the annual and seasonal mean responses are qualitatively relevant for
857 assessing air quality changes as measured by a threshold statistic used to gauge
858 compliance with air quality standards.

859 We define an “import sensitivity” as the ratio of the sum of the change in surface
860 O₃ resulting from perturbations to precursor emissions in the three foreign source regions
861 to the surface O₃ change resulting from the same perturbations to domestic emissions.
862 The model ensemble mean import sensitivity ranges from 0.5 (SA in November) to
863 1.1(EA in March) during the month with the largest surface O₃ response to the combined
864 foreign emission reductions. Regional O₃ production reaches a maximum in summer
865 over EA, EU, and NA (Figure 5), with model ensemble mean import sensitivities for July
866 of 0.2 (NA and EA) to 0.3 (EU). We assign a high degree of uncertainty, however, to the
867 NA and EA results given the model bias compared to surface observations during the
868 summer and early fall (Figure 2).

869 The responses to emission reductions of the traditional O₃ precursors from a
870 single foreign source region are often 10% (maximum of ~50%) of the responses to
871 domestic emission reductions. This foreign influence is not trivial if one considers that

872 application of the cheapest air pollution control measures in industrialized nations renders
873 additional controls disproportionately expensive [Keating *et al.*, 2004] and that our
874 results are large spatial averages that do not convey the larger foreign influence occurring
875 in some sub-continental regions (*e.g.* the west coasts of NA and EU). From the multi-
876 model ensemble mean response to a 20% decrease in global CH₄ abundances, we infer
877 that the O₃ decrease over foreign regions produced by regional reductions in
878 anthropogenic CH₄ emissions is roughly equivalent to the O₃ decrease from the same
879 percentage reduction of NO_x, NMVOC, and CO together. The inclusion of
880 anthropogenic CH₄ emissions as a strategy to decrease hemispheric O₃ may be
881 economically attractive given the availability of low-cost control measures [West and
882 Fiore, 2005]. From a perspective of jointly addressing climate and air quality, a multi-
883 species approach to reducing O₃ pollution is preferable to reducing NO_x alone [*e.g.*, Wild
884 *et al.*, 2001; Fuglestedt *et al.*, 1999, Naik *et al.* 2005; Shindell *et al.*, 2005]. Our results
885 provide a baseline for future assessments of intercontinental SR relationships. This
886 baseline is a key step towards informing air pollution managers confronted by the
887 possibility that future increases in global emissions could offset air quality improvements
888 attained via regulations on domestic emissions.

889

890

891 **Acknowledgments**

892 We are grateful to D. Jaffe and D. Reidmiller (University of Washington), and to A.
893 Gnanadesikan and R. Stouffer (GFDL) for insightful comments on draft versions of the
894 manuscript.

895

896 **References**

897

898 Akimoto, H. (2003), Global Air Quality and Pollution, *Science*, 302, 5651,1716-1719.

899

900 Auvray, M. and I. Bey, (2005), Long-range transport to Europe: Seasonal variations and
901 implications for the European ozone budget, *Journal of Geophysical Research*
902 110(D11303).

903

904 Bergin, M.S., J.J. West, T.J. Keating, A.G. Russell (2005), Regional Atmospheric
905 Pollution and Transboundary Air Quality Management, *Annu. Rev. Environ. Resour.*
906 30:1-37,doi: 10.1146/annurev.energy.30.050504.144138

907

908 Berntsen, T.K., S. Karlsdottir, and D.A. Jaffe (1999), Influence of Asian emissions on the
909 composition of air reaching the North Western United States, *Geophys. Res. Lett.* 26,
910 2172-2174.

911

912 Bey, I., D.J. Jacob, J.A. Logan, and R.M. Yantosca (2001), Asian chemical outflow to the
913 Pacific in spring: Origins, pathways, and budgets, *J. Geophys. Res.*, 106 (D19), 23,097-
914 23,113.

915

916 Bowman, K.P., and G.D. Carrie (2005), The Mean-Meridional Transport Circulation of
917 the Troposphere in an Idealized GCM, *J. Atmos. Sci.*, 59, 1502-1514.

918
919 Carslaw, D.C. (2005), On the changing seasonal cycles and trends of ozone at Mace Head
920 Ireland, *Atmos. Chem. Phys.*, 5, 3441-3450.
921
922 Cofala, J., M. Amann, Z. Klimont, and W. Schöpp (2005) Scenarios of World
923 Anthropogenic Emissions of SO₂, NO_x, and CO up to 2030, in Internal report of the
924 Transboundary Air Pollution Programme, pp. 17,
925 http://www.iiasa.ac.at/rains/global_emiss/global_emiss.html, International Institute for
926 Applied Systems Analysis, Laxenburg, Austria.
927
928 Collins, W.J., D. S. Stevenson, C. E. Johnson and R. G. Derwent (2000), The European
929 regional ozone distribution and its links with the global scale for the years 1992 and 2015
930 *Atmos. Environ.*, 34, 255-267.
931
932 Collins, W.J., R.G. Derwent, C.E. Johnson, and D.S. Stevenson (2002), The oxidation of
933 organic compounds in the troposphere and their global warming potentials, *Climatic*
934 *Change*, 52, 453-479.
935
936 Cooper, O. R., and J. L. Moody, Meteorological controls on ozone at an elevated eastern
937 United States regional background monitoring site, *J. Geophys. Res.*, 105, 6855– 6869,
938 2000.
939
940 Crutzen, P. (1973), A discussion of the chemistry of some minor constituents in the
941 stratosphere and troposphere, *Pure Appl. Geophys.*, 106-108, 1385-1399.
942
943 Daniel, J.S., and S. Solomon (1998) On the climate forcing of carbon monoxide, *J.*
944 *Geophys. Res.*, 103, 13,249-13,260.
945
946 Denman, K.L., et al. (2007), Couplings Between Changes in the Climate System and
947 Biogeochemistry. In: *Climate Change 2007: The Physical Science Basis, Contribution of*
948 *Working Group I to the Fourth Assessment Report of the Intergovernmental Panel on*
949 *Climate Change* [Solomon, S. and 7 others (eds.)]. Cambridge University Press,
950 Cambridge, United Kingdom and New York, NY, USA.
951
952 Dentener, F., D. Stevenson, J. Cofala, R. Mechler, M. Amann, P. Bergamaschi, F. Raes,
953 and R. Derwent (2005), The impact of air pollutant and methane emission controls on
954 tropospheric ozone and radiative forcing: CTM calculations for the period 1990-2030,
955 *Atmos. Chem. Phys.* 5, 1731-1755.
956
957 Dentener, F., et al. (2006), The global atmospheric environment for the next generation,
958 *Environ. Sci. Technol.*, 40, 3586-3594.
959
960 Derwent, R.G., P.G. Simmonds, S. Seuring, C. Dimmer (1998), Observation and
961 interpretation of the seasonal cycles in the surface concentrations of ozone and carbon
962 monoxide at Mace Head, Ireland from 1990 to 1994, *Atmos. Environ.*, 32 (2), 145-157.
963

964 Derwent, R.G., W.J. Collins, C.E. Johnson, and D.S. Stevenson (2001), Transient
965 behaviour of tropospheric ozone precursors in a global 3-D CTM and their indirect
966 greenhouse effects, *Climatic Change*, 39, 463-487.
967

968 Derwent, R. G., et al. (2002), Coupling between the global and regional scale ozone
969 distributions over Europe and the role of intercontinental transport, presented at the
970 USEPA/EMP workshop on hemispheric pollution.
971

972 Derwent, R.G., M.E. Jenkin, S.M. Saunders, M. J. Pilling, P.G. Simmonds, N.R. Passant,
973 G.J. Dollard, P. Dumitrean, A. Kent (2003), Photochemical ozone formation in north
974 west Europe and its control, *Atmos. Environ.* 37, 1983-1991.
975

976 Derwent, R. G., D. S. Stevenson, et al., (2004), Intercontinental transport and the origins
977 of the ozone observed at surface sites in Europe, *Atmospheric Environment* 38(13): 1891-
978 1901.
979

980 Derwent, R.G., P.G. Simmonds, S. O’Doherty, D.S. Stevenson, W.J. Collins, M.G.
981 Sanderson, C.E. Johnson, F. Dentener, J. Cofala, R. Mechler, M. Ammann (2006),
982 External influences on Europe’s air quality: Baseline methane, carbon monoxide and
983 ozone from 1990 to 2030 at Mace Head, Ireland, *Atmos. Environ.*, 40, 844-855.
984

985 Derwent, R.G., P.G. Simmonds, A.J. Manning, T.G. Spain (2007) Trends over a 20-year
986 period from 1987-2007 in surface ozone at the atmospheric research station, Mace Head,
987 Ireland, *Atmos. Environ.*, 41, 9091-9098.
988

989 Duncan, B.N., J.J. West, Y. Yoshida, A.M. Fiore, and J.R. Ziemke (2008), The
990 influence of European pollution on ozone in the Near East and northern
991 Africa, *Atmos. Chem. Phys.*, 8, 2267-2283.
992

993 Eckhardt, S., A. Stohl, H. Wernli, P. James, C. Forster, and N. Spichtinger (2004), A 15-
994 Year Climatology of Warm Conveyor Belts, *Journal of Climate*, 17 (1), pp. 218–237.
995

996 Ellingsen, K., M. Gauss, R. van Dingenen, F.J. Dentener, *et al.* (2008), Global ozone and
997 air quality: a multi-model assessment of risks to human health and crops, *Atmos. Chem.*
998 *Phys. Discuss.*, 8, 2163–2223, www.atmos-chem-phys-discuss.net/8/2163/2008/
999

1000 Fiore, A. M., D.J. Jacob, B.D. Field, D.G. Streets, S.D. Fernandes, and C. Jang (2002a),
1001 Linking Air Pollution and Climate Change: The Case for Controlling Methane, *Geophys.*
1002 *Res. Lett.* **29**, 1919.
1003

1004 Fiore, A.M., D.J. Jacob, I. Bey, R.M. Yantosca, B.D. Field, A.C. Fusco, and J.G.
1005 Wilkinson (2002b), Background ozone over the United States in summer: Origin,trend,
1006 and contribution to pollution episodes, *J. Geophys. Res.*, 107 (D15),
1007 doi:10.1029/2001JD000982.
1008

1009 Fiore, A., D. J. Jacob, H. Liu, R. M. Yantosca, T. D. Fairlie, and Q. Li (2003), Variability
1010 in surface ozone background over the United States: Implications for air quality policy, *J.*
1011 *Geophys. Res.*, *108(D24)*, 4787, doi:10.1029/2003JD003855.
1012

1013 Fiore, A. M., J. J. West, L. W. Horowitz, V. Naik, and M. D. Schwarzkopf (2008),
1014 Characterizing the tropospheric ozone response to methane emission controls and the
1015 benefits to climate and air quality, *J. Geophys. Res.*, *113*, D08307,
1016 doi:10.1029/2007JD009162
1017

1018 Frost G. J., et al. (2006), Effects of changing power plant NO_x emissions on ozone in the
1019 eastern United States: Proof of concept, *J. Geophys. Res.*, *111*, D12306,
1020 doi:10.1029/2005JD006354.
1021

1022 Fuglestedt, J. S., et al. (1999), Climatic forcing of nitrogen oxides through changes in
1023 tropospheric ozone and methane: Global model studies, *Atmos. Environ.*, *33*, 961–967.
1024

1025 Goldstein, A. H., D. B. Millet, et al., (2004), Impact of Asian emissions on observations
1026 at Trinidad Head, California, during ITCT 2k2, *Journal of Geophysical Research*
1027 *109(D23S17)*.
1028

1029 Guerova, G., I. Bey, J.-L. Attié, R. V. Martin, J. Cui, and M. Sprenger (2006), Impact of
1030 transatlantic transport episodes on summertime ozone in Europe, 2057-2072, SRef-ID:
1031 1680-7324/acp/2006-6-2057.
1032

1033 Han, Z., et al. (2008), MICS-Asia II: Model intercomparison and evaluation of ozone and
1034 relevant species, *Atmos. Environ.*, *42 (15)*, 3491-3509.
1035

1036 Hess, P. (2005), A comparison of two paradigms: The relative global roles of moist
1037 convective versus nonconvective transport, *J. Geophys. Res.*, *110*, D20302,
1038 doi:10.1029/2004JD005456.
1039

1040 Hess, P. and J.-F. Lamarque, (2007), Ozone source attribution and its modulation by the
1041 Arctic Oscillation during the spring months, *Journal of Geophysical Research*, *112*,
1042 D11303, doi:10.1029/2006JD007557.
1043

1044 Holloway, T., A. Fiore, and M. Galanter Hastings (2003), Intercontinental Transport of
1045 Air Pollution: Will emerging science lead to a new hemispheric treaty?, *Environ. Sci. &*
1046 *Technol.* , *37 (20)*, 4535-4542.
1047

1048 Holloway, T., C.C. Moberg, S. Ehlers (2007), Regional Variations in Intercontinental
1049 Transport of Ozone to the United States, *Eos Trans. AGU*, *88(52)*, Fall Meet. Suppl.,
1050 Abstract A43G-06.
1051

1052 Holloway, T., et al. (2008), MICS-Asia II: Impact of global emissions on regional air
1053 quality in Asia, *Atmos. Environ.*, *42 (15)*, 3543-3561.
1054

1055 Holzer, M., T.M. Hall, R.B. Stull (2005), Seasonality and weather-driven variability of
1056 transpacific transport, *J. Geophys. Res.*, 110, D23103, doi:10.1029/2005JD0006261.
1057
1058 Huntrieser H., et al. (2005), Intercontinental air pollution transport from North America
1059 to Europe: Experimental evidence from airborne measurements and surface observations,
1060 *J. Geophys. Res.*, 110, D01305, doi:10.1029/2004JD005045.
1061
1062 Husar, R., et al. (2001), Asian dust events of April 1998, *J. Geophys. Res.*, 106(D16),
1063 18317-18330.
1064
1065 Jacob, D.J., L.W. Horowitz, J.W. Munger, B.G. Heikes, R.R. Dickerson, R.S. Artz, and
1066 W.C. Keene (1995), Seasonal transition from NO_x- to hydrocarbon-limited conditions for
1067 ozone production over the eastern United States in September, *J. Geophys. Res.*, 100,
1068 9315-9324.
1069
1070 Jacob, D.J., J.A. Logan, and P.P. Murti (1999), Effect of rising Asian emissions on
1071 surface ozone in the United States, *Geophys. Res. Lett.*, 26, 2175-2178.
1072
1073 Jaeglé L., Jaffe D.A., Price H.U., Weiss-Penzias P., Palmer P.I., Evans M.J., Jacob D.J.,
1074 and Bey I (2003), Sources and budgets for CO and O₃ in the Northeast Pacific during the
1075 spring of 2001: Results from the PHOBEA-II Experiment, *J. Geophys. Res.* 108 (D20),
1076 8802, doi: 10.1029/2002JD003121.
1077
1078 Jaffe D.A., Anderson T., Covert D., Kotchenruther R., Trost B., Danielson J., Simpson
1079 W., Berntsen T., Karlsdottir S. Blake D., Harris J., Carmichael G. and Uno I. (1999)
1080 Transport of Asian Air Pollution to North America. *Geophys. Res. Lett.* 26, 711-714.
1081
1082 Jaffe D., Snow J., and Cooper O. (2003a), The April 2001 Asian dust events: Transport
1083 and substantial impact on surface particulate matter concentrations across the United
1084 States. *EOS transactions*. Nov. 18th.
1085
1086 Jaffe, D.; McKendry, I.; Anderson, T.; Price H. (2003b), Six 'New' Episodes of Trans-
1087 Pacific Transport of Air Pollutants; *Atmos. Environ.* 37, 391-404.
1088
1089 Jaffe, D. A., D. Parrish, et al., (2003c), Increasing background ozone during spring on the
1090 west coast of North America, *Geophys. Res. Lett.* 30(12): 1613.
1091
1092 Jaffe, D., I. Bertsch, L. Jaeglé, P. Novelli, J. S. Reid, H. Tanimoto, R. Vingarzan, and
1093 D.L. Westphal (2004), Long-range transport of Siberian biomass burning emissions and
1094 impact on surface ozone in western North America, *Geophys. Res. Lett.*, 31, L16106,
1095 doi:10.1029/2004GL020093.
1096
1097 Jaffe, D., and J. Ray (2007), Increase in surface ozone at rural sites in the western US,
1098 *Atmos. Environ.*, 41, 5452–5463.
1099

1100 Jaffe D.A., Hafner W., Chand D., Westerling A., Spracklen D. (2008), Influence of Fires
1101 on O₃ Concentrations in the Western U.S. In press., *Envir.Sci.Tech.*, April 2008.
1102

1103 Jonson, J. E., Simpson, D., Fagerli, H., and Solberg, S. (2005). Can we explain the trends
1104 in European ozone levels? *Atmospheric Chemistry and Physics*, 6(1), 51-66
1105

1106 Keating, T. J., West, J. J. & Farrell, A. E. (2004) in *Intercontinental Transport
1107 of Air Pollution*, ed. Stohl, A. (Springer, Berlin), pp. 295–320.
1108

1109 Kunhikrishnan, T., M.G. Lawrence, R. von Kuhlmann, M.O. Wenig, A.H.Asman, A.
1110 Richter, and J.P. Burrows (2006), Regional NO_x emission strength for the Indian
1111 subcontinent and the impact of emissions from India and neighboring countries on
1112 regional O₃ chemistry, *J. Geophys. Res.*, 111, D15301, doi:10.1029/2005JD006036.
1113

1114 Lamarque, J.-F. and P. Hess (2004), Arctic Oscillation modulation of the Northern
1115 Hemisphere spring tropospheric ozone, *Geophys. Res. Lett.*, 31, L06127,
1116 doi:10.1029/2003GL019116.
1117

1118 Lelieveld, J. et al. (2002a), Global Air Pollution Corssroads over the Mediterranean,
1119 *Science*, 298, 794-799, doi:10.1126/science.1075457.
1120

1121 Lelieveld, J., W. Peters, F.J. Dentener, and M.C. Krol (2002b), Stability of tropospheric
1122 hydroxyl chemistry, *J. Geophys. Res.*, D23, 10.1029/2002JD002272.
1123

1124 Li, Q.B., et al. (2001), A tropospheric ozone maximum over the Middle East, *Geophys.
1125 Res. Lett.*, 28, 3235-3238.
1126

1127 Li, Q., et al. (2002), Transatlantic transport of pollution and its effects on surface ozone
1128 in Europe and North America, *J. Geophys. Res.*, 107, 4166, 10.1029/2001JD001422.
1129

1130 Liang, Q., L. Jaeglé, and J. M. Wallace (2005), Meteorological indices for Asian outflow
1131 and transpacific transport on daily to interannual timescales, *J. Geophys. Res.*, 110,
1132 D18308, doi:10.1029/2005JD005788.
1133

1134 Lin, J.-T., D. J. Wuebbles, and X.-Z. Liang (2008), Effects of intercontinental transport
1135 on surface ozone over the United States: Present and future assessment with a global
1136 model, *Geophys. Res. Lett.*, 35, L02805, doi:10.1029/2007GL031415.
1137

1138 Liu, H., D.J. Jacob, L.Y. Chan, S.J. Oltmans, I. Bey, R.M. Yantosca, J.M. Harris, B.N.
1139 Duncan, and R.V. Martin, Sources of tropospheric ozone along the Asian Pacific Rim:
1140 An analysis of ozonesonde observations (2002), *J. Geophys. Res.*, 107 (D21),
1141 4573,10.1029/2001JD002005.
1142

1143 Liu, H.; Jacob, D.J.; Bey, I.; Yantosca, R.M.; Duncan, B.N.; Sachse G.W. Transport
1144 Pathways for Asian Pollution Outflow over the Pacific: Interannual and Seasonal
1145 Variations (2003), *J. Geophys. Res.*, 108, 8786.

1146
1147 Liu, J., D. L. Mauzerall, and L. W. Horowitz (2005), Analysis of seasonal and
1148 interannual variability in transpacific transport, *J. Geophys. Res.*, 110, D04302,
1149 doi:10.1029/2004JD005207.

1150
1151 Logan, J.A. (1999), An Analysis of Ozonesonde Data for the Troposphere:
1152 Recommendations for Testing 3-D Models, and Development of a Gridded Climatology
1153 for Tropospheric Ozone, *J. Geophys. Res.*, 104, 16115-16149.

1154
1155 Naik, V., D. Mauzerall, L. Horowitz, M. D. Schwarzkopf, V. Ramaswamy, and M.
1156 Oppenheimer (2005), Net radiative forcing due to changes in regional emissions of
1157 tropospheric ozone precursors, *J. Geophys. Res.*, 110, D24306,
1158 doi:10.1029/2005JD005908.

1159
1160 Olivier, J. G. J., et al. (2005), Recent trends in global greenhouse gas emissions: Regional
1161 trends and spatial distribution of key sources, in *Non-CO2 Greenhouse Gases (NCGG-4)*,
1162 edited by A. van Amstel, pp. 325– 330, Millpress, Rotterdam, Netherlands.

1163
1164 Oltmans et al. (2006), Long-term changes in tropospheric ozone, *Atmos. Environ.*, 40,
1165 3156-3173.

1166
1167 Ordóñez, C., D. Brunner, J. Staehelin, P. Hadjinicolaou, J. A. Pyle, M. Jonas, H. Wernli,
1168 and A. S. H. Prévôt (2007), Strong influence of lowermost stratospheric ozone on lower
1169 tropospheric background ozone changes over Europe, *Geophys. Res. Lett.*, 34, L07805,
1170 doi:10.1029/2006GL029113.

1171
1172 Parrish D. D., et al. (2004), Changes in the photochemical environment of the temperate
1173 North Pacific troposphere in response to increased Asian emissions, *J. Geophys. Res.*,
1174 109, D23S18, doi:10.1029/2004JD004978.

1175
1176 Prather, M. J. (1996), Time scales in atmospheric chemistry: Theory, GWPs for CH₄ and
1177 CO, and runaway growth, *Geophys. Res. Lett.*, 23, 2597-2600.

1178
1179 Prather, M., et al. (2001), in *Climate Change 2001: The Scientific Basis*, eds. Houghton,
1180 J. T., Ding, Y., Griggs, D. J., Noguer, M., van der Linden, P. J., Dai, X., Maskell, K. &
1181 Johnson, C. A. (Cambridge University Press, Cambridge), pp. 239-287.

1182
1183 Prospero, J. M. (1999), Long-term measurements of the transport of African mineral dust
1184 to the southeastern United States: Implications for regional air quality, *Journal of*
1185 *Geophysical Research-Atmospheres* 104(D13): 15917-15927.

1186
1187 Pochanart P., H. Akimoto, Y. Kajii, V. M. Potemkin, and T. V. Khodzher (2003),
1188 Regional background ozone and carbon monoxide variations in remote Siberia/East Asia,
1189 *J. Geophys. Res.*, 108 (D1), 4028, doi:10.1029/2001JD001412.

1190

1191 Reichler, T., and J. Kim (2008), How Well do Coupled Models Simulate Today's
1192 Climate?, *Bull. Amer. Meteor. Soc.*, 89, 303-311.
1193
1194 Richter, A., J. P. Burrows, et al., (2005), Increase in tropospheric nitrogen dioxide over
1195 China observed from space, *Nature* 437(7055): 129-132.
1196
1197 Sanderson, M., et al (2008), Oxidised Nitrogen Source-Receptor Relationships, submitted
1198 to *Geophys. Res. Lett.*.
1199
1200 Schultz, M.G., et al. (2007), REanalysis of the TROpospheric (RETRO) chemical
1201 composition over the past 40 years, Report no. 48/2007 in the series "Reports on Earth
1202 System Science" of the Max Planck Institute for Meteorology, Hamburg, ISSN 1614-
1203 1199.
1204
1205 Schulz, M., et al. (2006), Radiative forcing by aerosols as derived from the AeroCom
1206 present-day and pre-industrial simulations, *Atmos. Chem. Phys.*, 6, 5225-5246.
1207
1208 Shindell D. T., G. Faluvegi, N. Bell, G. A. Schmidt (2005), An emissions-based view of
1209 climate forcing by methane and tropospheric ozone, *Geophys. Res. Lett.*, 32, L04803,
1210 doi:10.1029/2004GL021900.
1211
1212 Shindell, D.T., G. Faluvegi, N. Unger, E. Aguilar, G. A. Schmidt, D. M. Koch, S. E.
1213 Bauer, and R. L. Miller (2006), Simulations of preindustrial, present-day, and 2100
1214 conditions in the NASA GISS composition and climate model G-PUCCINI, *Atmos.*
1215 *Chem. Phys.*, 6, 4427-4459.
1216
1217 Shindell, D. et al. (2008), A multi-model assessment of pollution transport to the Arctic,
1218 *Atmos. Chem. Phys. Disc.*, 8,8385.8429.
1219
1220 Sillman, S. (1999), The relation between ozone, NO_x and hydrocarbons in urban and
1221 polluted rural environments. Millennial Review series, *Atmos. Environ.*, 33, 12, 1821-
1222 1845.
1223
1224 Solberg, S., R.G. Derwent, O. Hov, J. Langner, and A. Lindskog (2005), European
1225 Abatement of Surface Ozone in a Global Perspective, *Ambio*, 34 (1), pp. 47-53.
1226
1227 Spivakovsky, C.M., et al. (2000), Three-dimensional climatological distribution of
1228 tropospheric OH: Update and evaluation, *J. Geophys. Res.*, 105 (D7), 8931-8980.
1229
1230 Stevenson, D.S., R.M. Doherty, M.G. Sanderson, W.J. Collins, C.E. Johnson, and R.G.
1231 Derwent (2004), Radiative forcing from aircraft NO_x emissions: Mechanisms and
1232 seasonal dependence, *J. Geophys. Res.*, 109, D17307, doi:10.1029/2004JD004759.
1233
1234 Stevenson, D.S., et al. (2006), Multi-model ensemble simulations of present-day and
1235 near-future tropospheric ozone, *J. Geophys. Res.*, 111, D08301,
1236 doi:10.1029/2005JD006338.

1237
1238 Stohl A., S. Eckhardt, C. Forster, P. James, and N. Spichtinger (2002), On the pathways
1239 and timescales of intercontinental air pollution transport, *J. Geophys. Res.*, 107 (D23),
1240 4684, doi:10.1029/2001JD001396.
1241
1242 Sudo K., H. Akimoto (2007), Global source attribution of tropospheric ozone: Long-
1243 range transport from various source regions, *J. Geophys. Res.*, 112, D12302,
1244 doi:10.1029/2006JD007992.
1245
1246 Szopa, S., et al., (2006), Future global tropospheric ozone changes and impact on
1247 European air quality, *Geophysical Research Letters* 33(L14805).
1248
1249 Task Force on Hemispheric Transport of Air Pollution (TF HTAP) (2007), Hemispheric
1250 Transport of Air Pollution 2007 Interim Report, Air Pollution Studies No. 16, T.J.
1251 Keating and A. Zuber (eds). United Nations Economic Commission for Europe, New
1252 York and Geneva, available at www.htap.org.
1253
1254 Trickl T., O. R. Cooper, H. Eisele, P. James, R. Mücke, A. Stohl (2003), Intercontinental
1255 transport and its influence on the ozone concentrations over central Europe: Three case
1256 studies, *J. Geophys. Res.*, 108 (D12), 8530, doi:10.1029/2002JD002735.
1257
1258 Vingarzan, R. (2004), A review of surface ozone background levels and trends, *Atmos.*
1259 *Environ.*, 38 (21), p.3431-3442.
1260
1261 Wang, Y., D.J. Jacob, and J.A. Logan (1998), *Global simulation of tropospheric O₃-NO_x-*
1262 *hydrocarbon chemistry, 3. Origin of tropospheric ozone and effects of non-methane*
1263 *hydrocarbons*, *J. Geophys. Res.*, 103/D9, 10,757-10,768.
1264
1265 Wang, Y., and D.J. Jacob (1998), Anthropogenic forcing on tropospheric ozone and OH
1266 since preindustrial times, *J. Geophys. Res.*, 103, 31,123-31,135.
1267
1268 Weiss-Penzias P., D. A. Jaffe, L. Jaeglé, Q. Liang (2004), Influence of long-range-
1269 transported pollution on the annual and diurnal cycles of carbon monoxide and ozone at
1270 Cheeka Peak Observatory, *J. Geophys. Res.*, 109, D23S14, doi:10.1029/2004JD004505.
1271
1272 Weiss-Penzias, P., D. A. Jaffe, P. Swartzendruber, J. B. Dennison, D. Chand, W. Hafner,
1273 and E. Prestbo (2006), Observations of Asian air pollution in the free troposphere at
1274 Mount Bachelor Observatory during the spring of 2004, *J. Geophys. Res.*,
1275 111, D10304, doi:10.1029/2005JD006522.
1276
1277 West, J.J., and A.M. Fiore (2005), Management of tropospheric ozone by reducing
1278 methane emissions , *Environ. Sci. & Technol.*, 39(13): 4685-4691,
1279 doi:10.1021/es048629f.
1280

1281 West, J. J., A. M. Fiore, V. Naik, L.W. Horowitz, M.D. Schwarzkopf, D.L. Mauzerall
1282 (2007a), Ozone air quality and radiative forcing consequences of changes in ozone
1283 precursor emissions, *Geophys. Res. Lett.*, *34*, L06806, 10.1029/2006GL029173.
1284
1285 Wild, O. and M.J.Prather (2000), Excitation of the primary tropospheric chemical mode
1286 in a global three-dimensional model, *J. Geophys. Res.*, *105 (D20)*, 24,647-24,660.
1287
1288 Wild, O. and H. Akimoto, (2001), Intercontinental transport of ozone and its precursors
1289 in a three dimensional globe CTM, *J. Geophys. Res.* *106(D21)*: 27729-27744.
1290
1291 Wild, O., M. J. Prather, and H. Akimoto (2001), Indirect long-term global radiative
1292 cooling from NO_x Emissions, *Geophys. Res.Lett.*, *28*, 1719– 1722.
1293
1294 Wild, O., P. Pochanart, et al., (2004), Trans-Eurasian transport of ozone and its
1295 precursors, *Journal of Geophysical Research* *109(D11302)*.
1296
1297 Wild, O., J.K. Sundet, M.J. Prather, I.S.A. Isaksen, H. Akimoto, E.V. Browell, and S.J.
1298 Oltmans (2003), CTM Ozone Simulations for Spring 2001 over the Western Pacific:
1299 Comparisons with TRACE-P lidar, ozonesondes and TOMS columns, *J. Geophys. Res.*,
1300 *108*, 8826, doi:10.1029/2002JD003283.
1301
1302 Wild, O. (2007), Modelling the global tropospheric ozone budget: exploring the
1303 variability in current models, *Atmos. Chem. Phys.*, *7*, 2643-2660.
1304
1305 Wilkening, K. E., L. A. Barrie, et al., (2000), Atmospheric Science: Trans-Pacific Air
1306 Pollution, *Science* *290(5489)*: 65-67.
1307
1308 World Health Organization (WHO), (2005), WHO air quality guidelines global update,
1309 report on a working group meeting, Bonn, Germany, 18-20 October, 2005, report number
1310 E87950.
1311
1312 Wu, S., L.J. Mickley, D.J. Jacob, J.A. Logan, R.M. Yantosca, and D. Rind (2007), Why
1313 are there large differences between models in global budgets of tropospheric ozone?, *J.*
1314 *Geophys. Res.*, *112*, D05302, doi:10.1029/2006JD007801.
1315
1316 Yienger, J., M. Galanter, T. Holloway, M. Phadnis, S. Guttikunda, G. Carmichael, W.
1317 Moxim, and H. Levy II (2000), The episodic nature of air pollution transport from Asia to
1318 North America, *J. Geophys. Res.*, *105(D22)*, 26931-26945.
1319
1320
1321

1322 **FIGURE CAPTIONS**

1323

1324 **Figure 1.** The HTAP source-receptor regions: NA (15-55°N; 60-125°W), EU (25-65°N;
1325 10°W-50°E) EA (15-50°N; 95-160°E), and SA (5-35°N; 50-95°E). Sites marked with
1326 the same symbols are used to produce the sub-regional averages in Figure 2, from the Co-
1327 operative programme for monitoring and evaluation of the long-range transmissions
1328 (EMEP) in the Mediteranean (red diamonds; panel a in Figure 2) and Central Europe
1329 (green open triangles for sites below 1 km and blue crosses for sites > 1 km; panels b and
1330 c in Figure 2, respectively); from the U.S. Clean Air Status and Trends Network
1331 (CASTNet) in the Northeast (red circles; panel d in Figure 2) Southwest (green triangles;
1332 e), Southeast (dark blue inverted triangles; f), Great Lakes (pink diamonds; g),
1333 Mountainous West (cyan squares; h), and from the Acid Deposition Monitoring Network
1334 in East Asia (EANET) in Japan (red asterisks; panel i in Figure 2).

1335

1336 **Figure 2.** Monthly mean surface O₃ concentrations (ppb) for the year 2001. Observed
1337 values (black circles) represent the average of all sites falling within the given latitude,
1338 longitude, and altitude boundaries and denoted by the colored symbols in Figure 1;
1339 vertical black lines depict the standard deviation across the sites. Monthly mean O₃ in the
1340 surface layer of the SR1 simulations from the 21 models are first sampled at the model
1341 grid cells containing the observational sites, and then averaged within sub-regions (grey
1342 lines); these spatial averages from each model are used to determine the multi-model
1343 ensemble median (solid red line) and mean (blue dashed line). Observations are from
1344 CASTNET (<http://www.epa.gov/castnet/ozone.html>) in the USA, from EMEP
1345 (<http://www.nilu.no/projects/ccc/emepdata.html>) in Europe, and from EANET
1346 (<http://www.eanet.cc/eanet.html>) in Japan.

1347

1348 **Figure 3.** Model ensemble surface O₃ response (ppb), annually and spatially averaged
1349 over the receptor regions (Figure 1) to 20% reductions of anthropogenic O₃ precursor
1350 emissions individually (NO_x, NMVOC, and CO), combined (ALL), and CH₄ within the
1351 source regions. Each group of bars includes results from the four regional perturbation
1352 experiments: NA (red), EU (green), EA (dark blue) and SA (cyan), as well as the sum of
1353 the impacts from the three foreign source regions (black bar). The responses to the global
1354 CH₄ level reduction are estimated as described in Section 5.3 using the model ensemble
1355 mean results from SR2-SR1 in Table A4) as well as the sum of the impacts from the three
1356 foreign source regions. The bars denote the multi-model mean response (colored by
1357 source region; see also Table A4) and the whiskers span the full range of the individual
1358 model responses.

1359

1360 **Figure 4.** Change in monthly mean surface O₃ over the receptor regions (one per panel)
1361 resulting from 20% decreases in domestic anthropogenic O₃ precursor emissions within
1362 that region: NO_x (SR3-SR1; red), VOC (SR4-SR1; green), CO (SR5-SR1; blue) and
1363 combined (ALL; SR6-SR1; black). Model ensemble means are shown for all available
1364 model results (filled circles; see Table A4 for the number of models contributing to each
1365 simulation) and for the subset of models in Table 2 (solid lines). The dotted line shows
1366 the model ensemble mean total O₃ response for the models in Table 2 (using all available
1367 simulations although not all models conducted every simulation) after accounting for the

1368 long-term impact from changes in CH₄ (see Section 5.2 for details) and shows little
1369 change from the short-term results.

1370
1371 **Figure 5.** Same as Figure 4, but for the sum of the O₃ responses to 20% decreases in
1372 anthropogenic emissions in the three foreign source regions.

1373
1374 **Figure 6.** Contribution of the three foreign source regions (colored lines) to the change in
1375 15-model monthly mean surface O₃ over the receptor regions (one per panel) resulting
1376 from combined 20% decreases in all anthropogenic O₃ precursor emissions (SR6-SR1;
1377 the black line for “ALL” is identical to the black circles in Figure 5).

1378
1379 **Figure 7.** Monthly mean import sensitivities for each region (IS_r; where r = NA (red), EU
1380 (green), EA (blue) and SA (cyan)), calculated as described in Section 4.1. Small
1381 wintertime domestic responses result in values >2 for IS_{NA} and IS_{EU} in the winter months,
1382 except for IS_{EU} in December and January which are negative due to O₃ titration from EU
1383 NO_x emissions (Figure 4).

1384
1385 **Figure 8.** Multi-model average decrease in surface O₃ over the receptor regions resulting
1386 from 20% reductions in the O₃ precursor emissions in the three foreign source regions
1387 (top panel) and in the domestic source region (bottom panel) for the season of peak
1388 sensitivity to those emissions (determined from Figures 5 and 4, respectively) in those
1389 models where aerosol emission reductions are not included in SR6 (FRGSC/UCI,
1390 GEMAQ-v1p0, STOC-HadAM3-v01, and UM-CAM-v01). To estimate the foreign
1391 influence, we assume linearity in the response to the individual source regions, with each
1392 color representing a summation of the model ensemble mean responses to the emission
1393 perturbations in the three foreign source regions.

1394
1395 **Figure 9.** Change in surface O₃ over the EU (left) and NA (right) as a function of
1396 various size perturbations to EU anthropogenic NO_x emissions by season (colors), as
1397 simulated with the FRSGC/UCI model (solid lines with circles) and as estimated by
1398 scaling linearly from the response in the simulation where NO_x emissions were decreased
1399 by 20% (SR3EU; dotted lines).

1400
1401 **Figure 10.** Decrease in annual mean NA surface O₃ (ppb) resulting from 20% reductions
1402 in EU anthropogenic NMVOC emissions (SR1-SR4EU) plotted against the EU
1403 anthropogenic NMVOC emissions (Tg C a⁻¹). The points represent the results from
1404 individual models (EU NMVOC emissions are given in Table A3). The coefficient of
1405 determination (r²) is 0.50.

1406
1407 **Figure 11.** Annual and seasonal mean contribution to total surface O₃ from foreign
1408 source regions as estimated from the individual model results in this study (colored by
1409 source region: green for EU; blue for EA, grey for EA+EU; red for NA) and from studies
1410 in the published literature (thin vertical bars for range across studies and regions; squares
1411 where one value is reported; note that regional definitions, methods for source attribution,
1412 and reported metrics (e.g. 24-hour vs. afternoon vs. daytime mean) vary across studies)
1413 [*Derwent et al.*, 1998; *Berntsen et al.*, 1999; *Wild and Akimoto*, 2001; *Derwent et al.*,

1414 2002; Fiore et al., 2002b; Jaeglé et al., 2003; Li et al., 2002; Liu et al., 2002; Pochanart
1415 et al., 2003; Derwent et al., 2004; Wild et al., 2004; Auvray and Bey, 2005; Guerova et
1416 al., 2006; Sudo and Akimoto, 2007; Duncan et al., 2008; Holloway et al., 2008; Lin et al.,
1417 2008, with all results scaled to 100% contributions as in Table 5-2 of *TF HTAP*, 2007].
1418 The contributions from this work are estimated by linearly scaling the simulated surface
1419 O₃ response to the combined 20% decreases in anthropogenic emissions of NO_x, CO, and
1420 NMVOC in the foreign source regions to 100% decreases, *i.e.*, 5*(SR1-SR6). The white
1421 circles represent the multi-model median value.

1422
1423 **Figure 12:** Observed (black circles) and simulated (grey diamonds) annual number of
1424 days when daily maximum 8-hour average O₃ concentrations exceed 60 ppb at the EMEP
1425 stations, averaged over the regions in Figure 2: Mediterranean (Medit.), Central European
1426 sites below 1 km altitude (C EU < 1km) and above 1 km altitude (C EU > 1km). The
1427 black vertical bars depict the standard deviation of the observed values across the stations
1428 within the region. The model ensemble mean (red circles) and median (green circles)
1429 values from the 18 models that contributed hourly surface O₃ results for SR1 are also
1430 shown.

1431
1432 **Figure 13.** As in Figure 6 but for the model ensemble mean change in the number of days
1433 per month when daily maximum 8-hour average O₃ concentrations exceed 60 ppb,
1434 spatially averaged within each receptor region (panels). The change is estimated by first
1435 calculating the area-weighted spatial average value for DAYS>60 in each model
1436 simulation for a given region (the right axis shows DAYS>60 in the base case, SR1), and
1437 then taking the multi-model average of the differences in the spatial average DAYS>60
1438 values (SR6-SR1) from the 12 models that provided hourly surface O₃ results for SR6.
1439
1440

1441 **Table 1.** Model ensemble annual mean (median) \pm one standard deviation in total and
 1442 anthropogenic emissions of NO_x (Tg N a⁻¹), NMVOC (Tg C a⁻¹), and CO (Tg a⁻¹),
 1443 globally and for the regions in Figure 1. Emissions in individual models are provided in
 1444 Tables A1 and A2.

Total Emis.	GLOBAL	NA	EU	EA	SA
NO _x	46.5(46.2) \pm 5.7	8.5(8.7) \pm 0.8	8.4(8.4) \pm 1.1	7.1(6.9) \pm 1.4	3.3(3.3) \pm 0.5
NMVOC	630(623) \pm 221	62(57) \pm 24	37(34) \pm 13	48(47) \pm 14	33(34) \pm 8.8
CO	1060(1090) \pm 135	130(130) \pm 20	90(81) \pm 25	150(150) \pm 29	97(96) \pm 23
Anthr. Emis.					
NO _x	32.5(29.4) \pm 6.0	7.4(7.3) \pm 0.4	7.3(7.5) \pm 0.6	6.0(5.5) \pm 1.4	2.4(2.2) \pm 0.4
NMVOC	96.8(92.3) \pm 41.8	16(16) \pm 7.0	19(20) \pm 11	16(17) \pm 6.5	10(10) \pm 3.9
CO	661(563) \pm 214	101(103) \pm 19	80(70) \pm 23	133(123) \pm 35	80(79) \pm 18

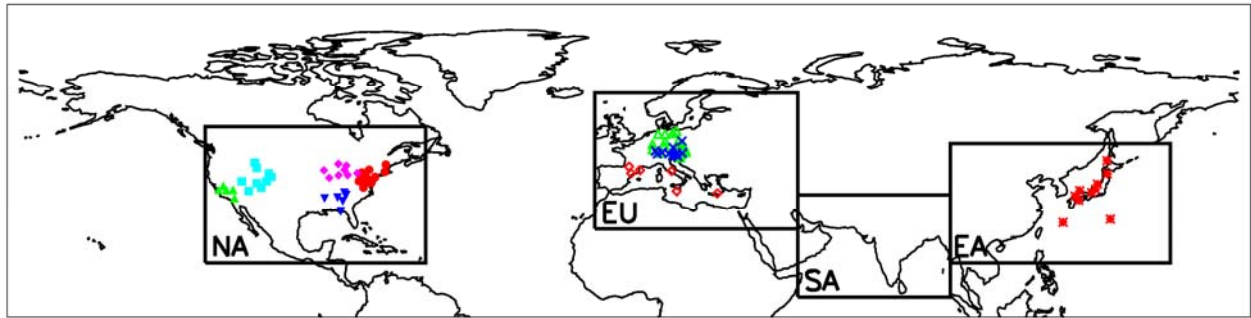
1445
 1446 **Table 2.** Methane lifetime (τ) and “feedback factor” (F) in the individual models
 1447

MODEL	τ_{OH}^a	τ_{tot}^b	F ^c
CAMCHEM-3311m13	11.86	10.11	1.30
FRSGUCI-v01	8.70	7.72	1.43
GISS-PUCCINI_modelE	10.88	9.39	1.36
GMI-v02f	10.38	9.02	1.31
LMDz3-INCA1	10.02	8.74	1.31
LLNL_IMPACT-T5a	6.19	5.68	1.40
MOZARTGFDL-v2	10.44	9.06	1.31
MOZECH-v16	11.20	9.63	1.29
STOCHEM-HadGEM	11.72	10.01	1.28
TM5-JRC-cy2-ipcc-v1	9.02	7.97	1.43
UM-CAM-v01	12.50	10.57	1.25
Model Ensemble Mean	10.26	8.90	1.33
Standard Deviation	1.78	1.38	0.06

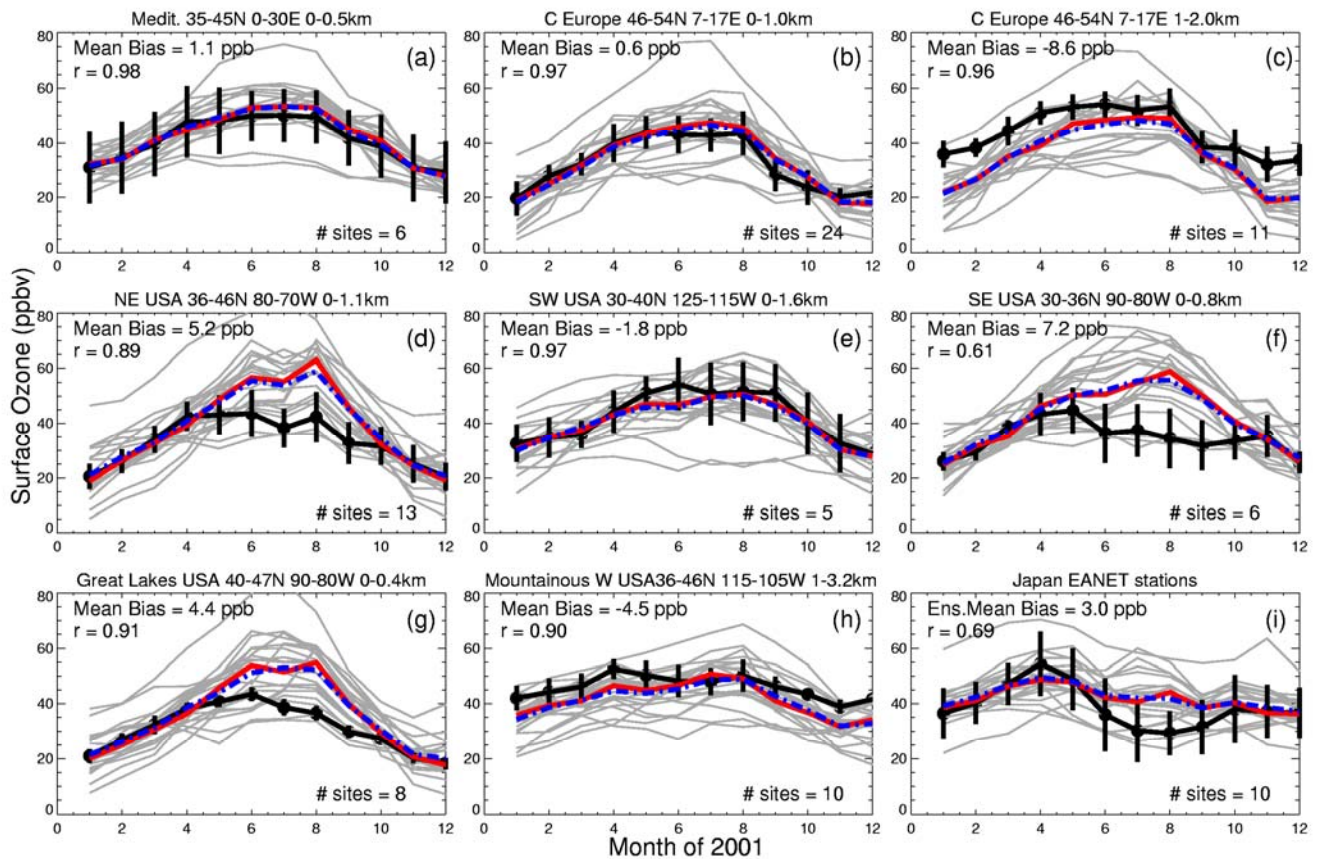
1448
 1449 ^a The methane lifetime against loss by tropospheric OH (years), defined as the total
 1450 atmospheric burden divided by the tropospheric CH₄ loss rates, with the troposphere
 1451 defined using the 150 ppb O₃ chemical tropopause.

1452 ^b τ = total atmospheric CH₄ lifetime (years) determined from τ_{OH} and assuming CH₄
 1453 losses to soils and the stratosphere with lifetimes of 160 and 120 years [Prather *et al.*,
 1454 2001], respectively.

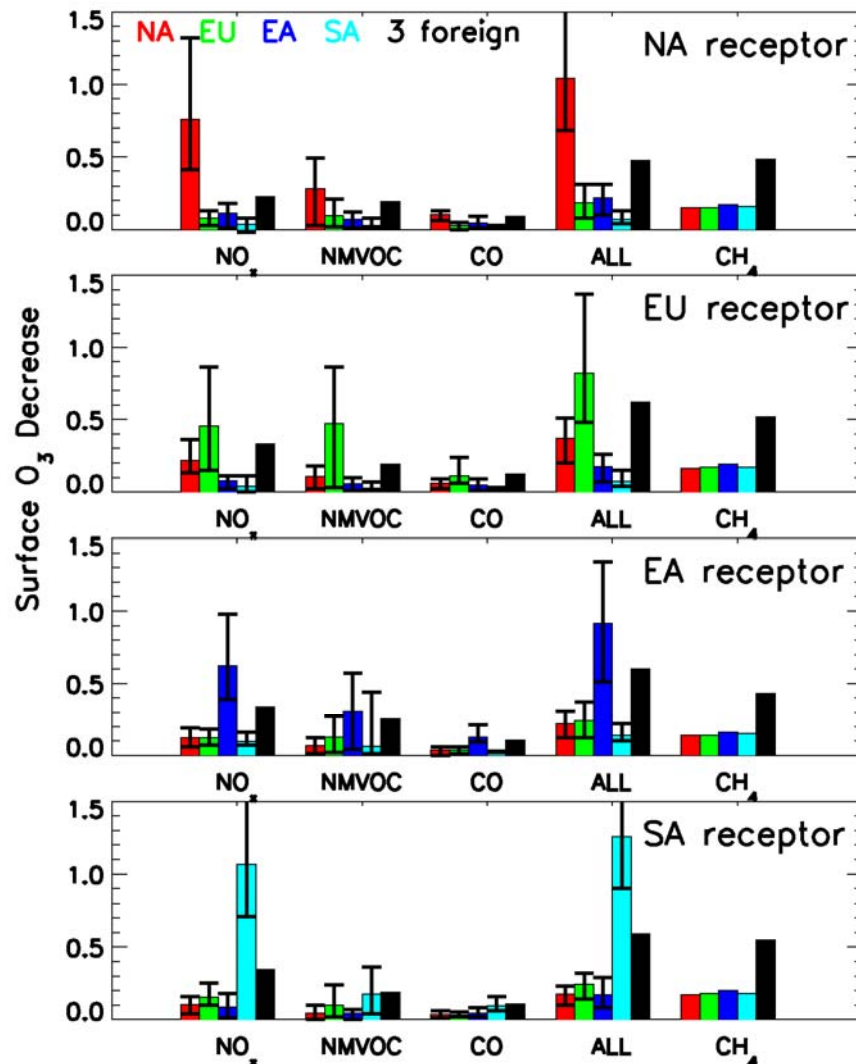
1455 ^cThe feedback factor is the ratio of the atmospheric response (or perturbation) time to the
 1456 global atmospheric lifetime and is given by $1/(1-s)$ where s is determined from the SR2
 1457 and SR1 simulations, and defined as $\delta \ln(\tau) / \delta \ln[CH_4]$ [Prather *et al.*, 2001], where
 1458 $[CH_4] = 1760$ ppb in SR1 and 1408 ppb in SR2.



1460
 1461 **Figure 1.** The HTAP source-receptor regions: NA (15-55°N; 60-125°W), EU (25-65°N;
 1462 10°W-50°E) EA (15-50°N; 95-160°E), and SA (5-35°N; 50-95°E). Sites marked with
 1463 the same symbols are used to produce the sub-regional averages in Figure 2, from the Co-
 1464 operative programme for monitoring and evaluation of the long-range transmissions
 1465 (EMEP) in the Mediterannean (red diamonds; panel a in Figure 2) and Central Europe
 1466 (green open triangles for sites below 1 km and blue crosses for sites > 1 km; panels b and
 1467 c in Figure 2, respectively); from the U.S. Clean Air Status and Trends Network
 1468 (CASTNet) in the Northeast (red circles; panel d in Figure 2) Southwest (green triangles;
 1469 e), Southeast (dark blue inverted triangles; f), Great Lakes (pink diamonds; g),
 1470 Mountainous West (cyan squares; h), and from the Acid Deposition Monitoring Network
 1471 in East Asia (EANET) in Japan (red asterisks; panel i in Figure 2).

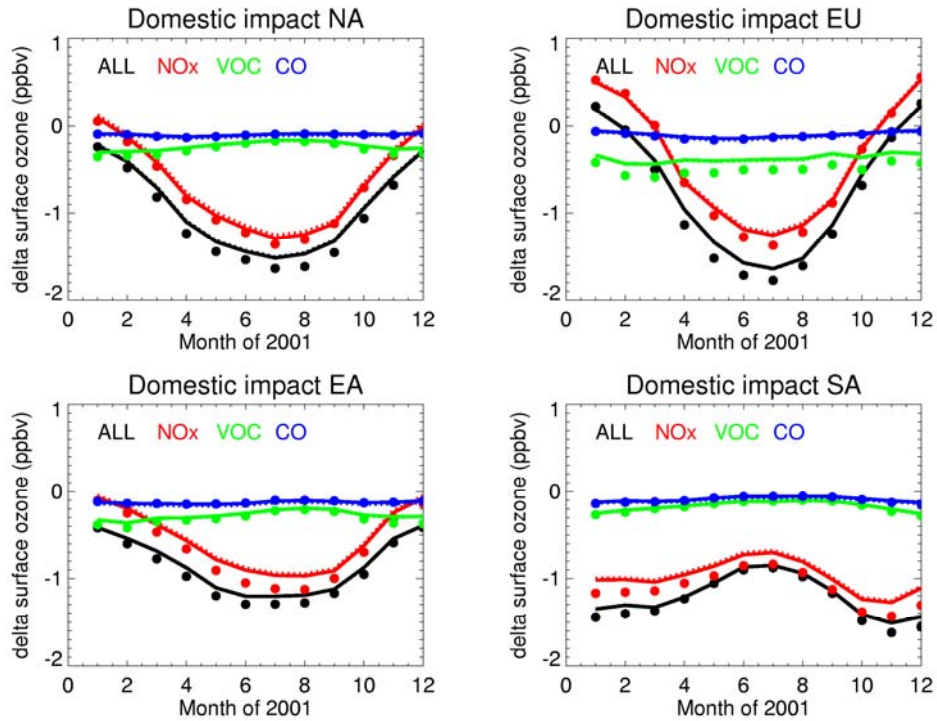


1473 **Figure 2.** Monthly mean surface O₃ concentrations (ppb) for the year 2001. Observed
 1474 values (black circles) represent the average of all sites falling within the given latitude,
 1475 longitude, and altitude boundaries and denoted by the colored symbols in Figure 1;
 1476 vertical black lines depict the standard deviation across the sites. Monthly mean O₃ in the
 1477 surface layer of the SR1 simulations from the 21 models are first sampled at the model
 1478 grid cells containing the observational sites, and then averaged within sub-regions (grey
 1479 lines); these spatial averages from each model are used to determine the multi-model
 1480 ensemble median (solid red line) and mean (blue dashed line). Observations are from
 1481 CASTNET (<http://www.epa.gov/castnet/ozone.html>) in the USA, from EMEP
 1482 (<http://www.nilu.no/projects/ccc/emepdata.html>) in Europe, and from EANET
 1483 (<http://www.eanet.cc/eanet.html>) in Japan.

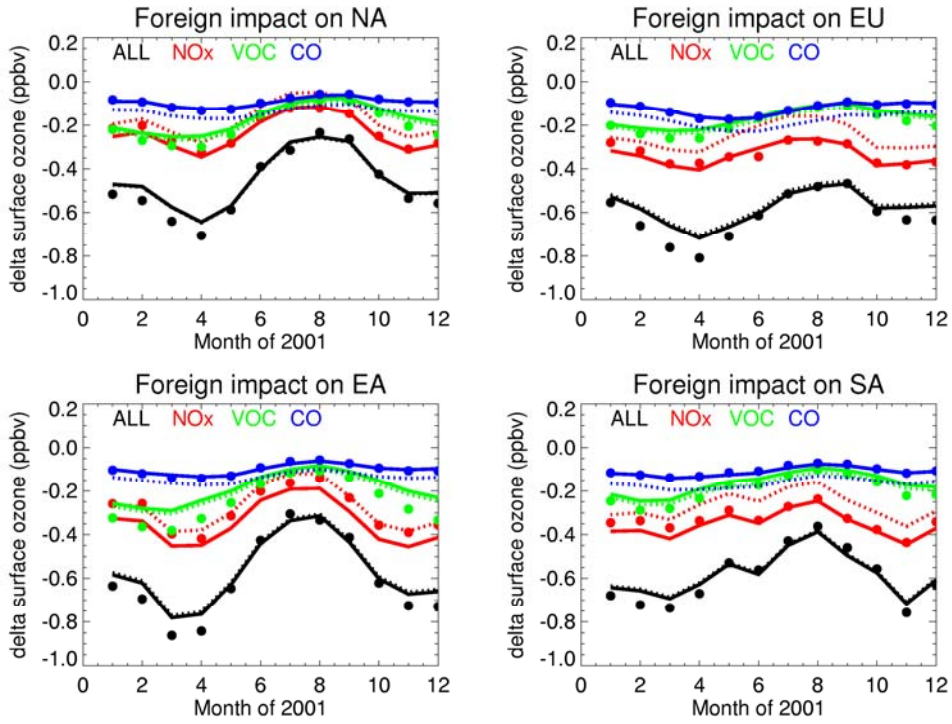


1484 **Figure 3.** Model ensemble surface O₃ response (ppb), annually and spatially averaged
 1485 over the receptor regions (Figure 1) to 20% reductions of anthropogenic O₃ precursor
 1486 emissions individually (NO_x, NMVOC, and CO), combined (ALL), and CH₄ within the
 1487 source regions. Each group of bars includes results from the four regional perturbation
 1488 experiments: NA (red), EU (green), EA (dark blue) and SA (cyan), as well as the sum of
 1489 the impacts from the three foreign source regions (black bar). The responses to the global
 1490

1491 CH₄ level reduction are estimated as described in Section 5.3 using the model ensemble
 1492 mean results from SR2-SR1 in Table A4) as well as the sum of the impacts from the three
 1493 foreign source regions. The bars denote the multi-model mean response (colored by
 1494 source region; see also Table A4) and the whiskers span the full range of the individual
 1495 model responses.
 1496

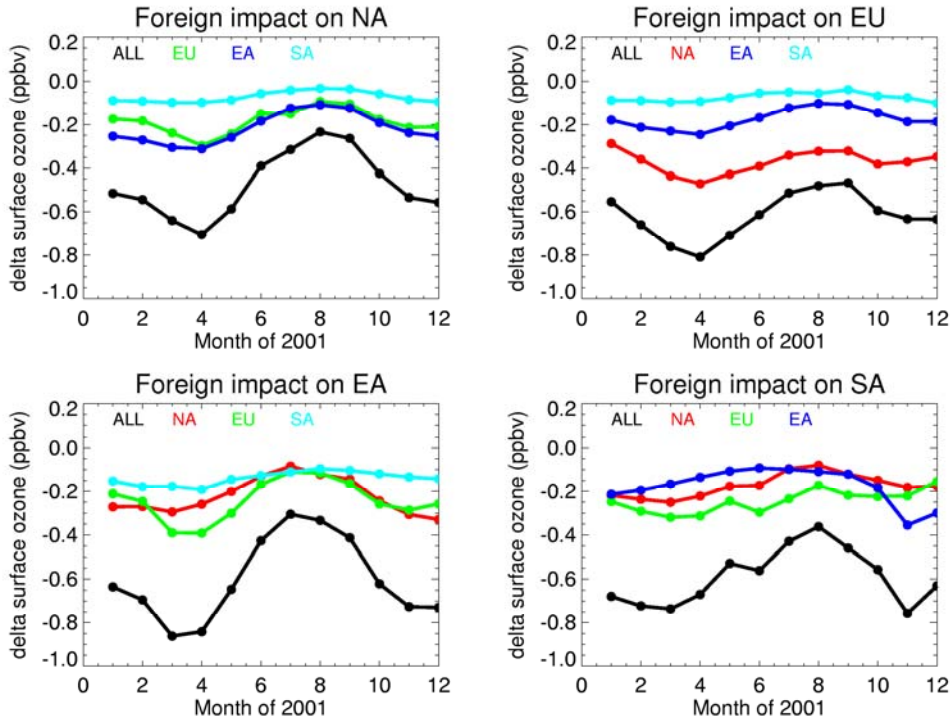


1497
 1498 **Figure 4.** Change in monthly mean surface O₃ over the receptor regions (one per panel)
 1499 resulting from 20% decreases in domestic anthropogenic O₃ precursor emissions within
 1500 that region: NO_x (SR3-SR1; red), VOC (SR4-SR1; green), CO (SR5-SR1; blue) and
 1501 combined (ALL; SR6-SR1; black). Model ensemble means are shown for all available
 1502 model results (filled circles; see Table A4 for the number of models contributing to each
 1503 simulation) and for the subset of models in Table 2 (solid lines). The dotted line shows
 1504 the model ensemble mean total O₃ response for the models in Table 2 (using all available
 1505 simulations although not all models conducted every simulation) after accounting for the
 1506 long-term impact from changes in CH₄ (see Section 5.2 for details) and shows little
 1507 change from the short-term results.



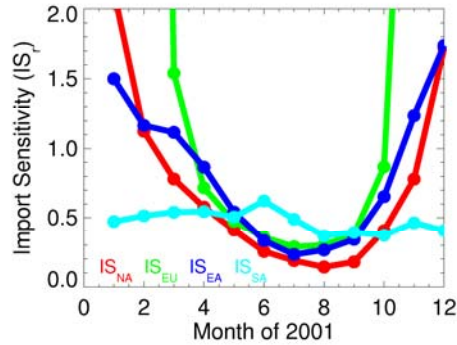
1508
 1509
 1510
 1511
 1512

Figure 5. Same as Figure 4, but for the sum of the O₃ responses to 20% decreases in anthropogenic emissions in the three foreign source regions.

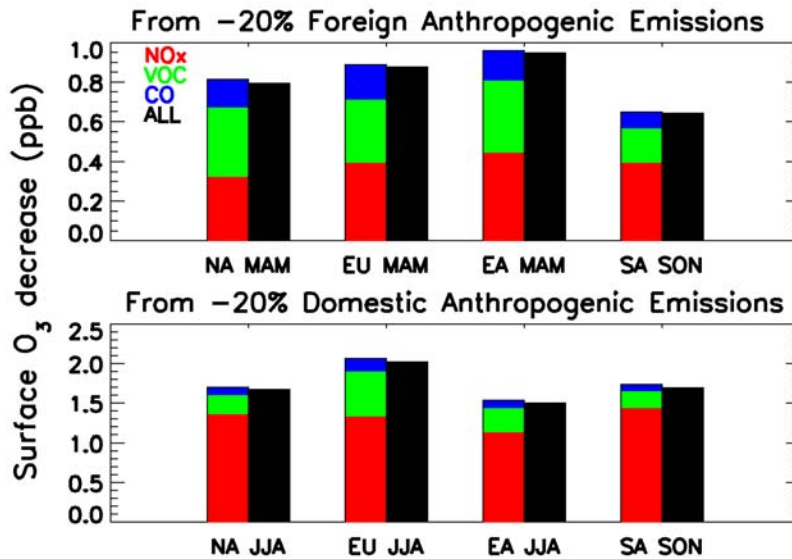


1513
 1514

1515 **Figure 6.** Contribution of the three foreign source regions (colored lines) to the change in
 1516 15-model monthly mean surface O₃ over the receptor regions (one per panel) resulting
 1517 from combined 20% decreases in all anthropogenic O₃ precursor emissions (SR6-SR1;
 1518 the black line for “ALL” is identical to the black circles in Figure 5).
 1519

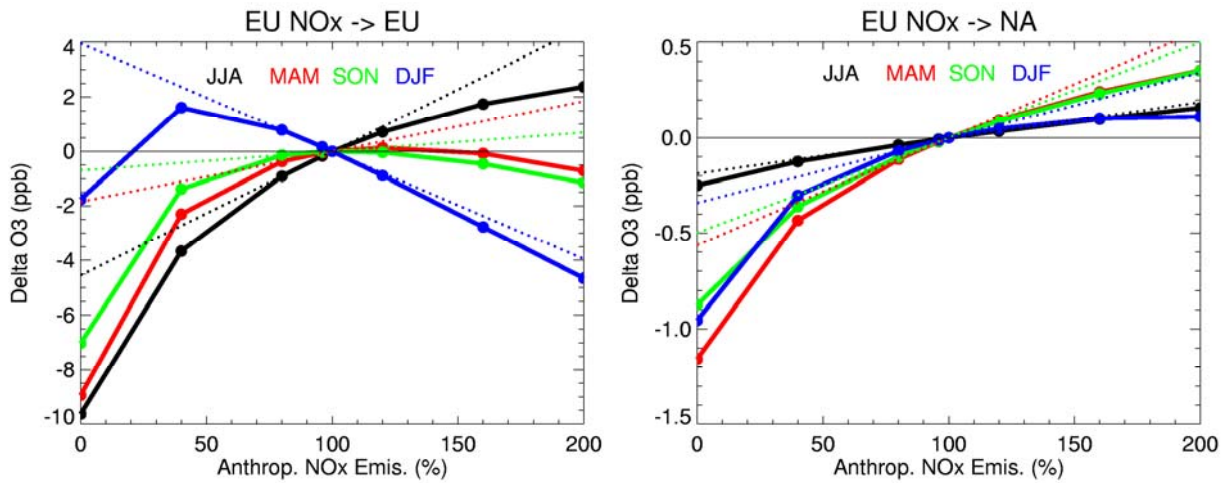


1520 **Figure 7.** Monthly mean import sensitivities for each region (IS_r; where r = NA (red), EU
 1521 (green), EA (blue) and SA (cyan)), calculated as described in Section 4.1. Small
 1522 wintertime domestic responses result in values >2 for IS_{NA} and IS_{EU} in the winter months,
 1523 except for IS_{EU} in December and January which are negative due to O₃ titration from EU
 1524 NO_x emissions (Figure 4).
 1525
 1526



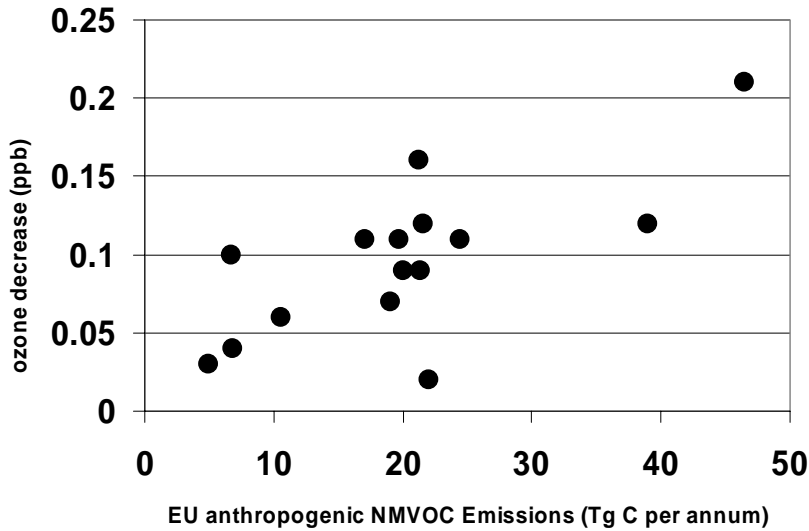
1527 **Figure 8.** Multi-model average decrease in surface O₃ over the receptor regions resulting
 1528 from 20% reductions in the O₃ precursor emissions in the three foreign source regions
 1529 (top panel) and in the domestic source region (bottom panel) for the season of peak
 1530 sensitivity to those emissions (determined from Figures 5 and 4, respectively) in those
 1531 models where aerosol emission reductions are not included in SR6 (FRGSC/UCI,
 1532 GEMAQ-v1p0, STOC-HadAM3-v01, and UM-CAM-v01). To estimate the foreign
 1533 influence, we assume linearity in the response to the individual source regions, with each
 1534 color representing a summation of the model ensemble mean responses to the emission
 1535 perturbations in the three foreign source regions.
 1536

1537



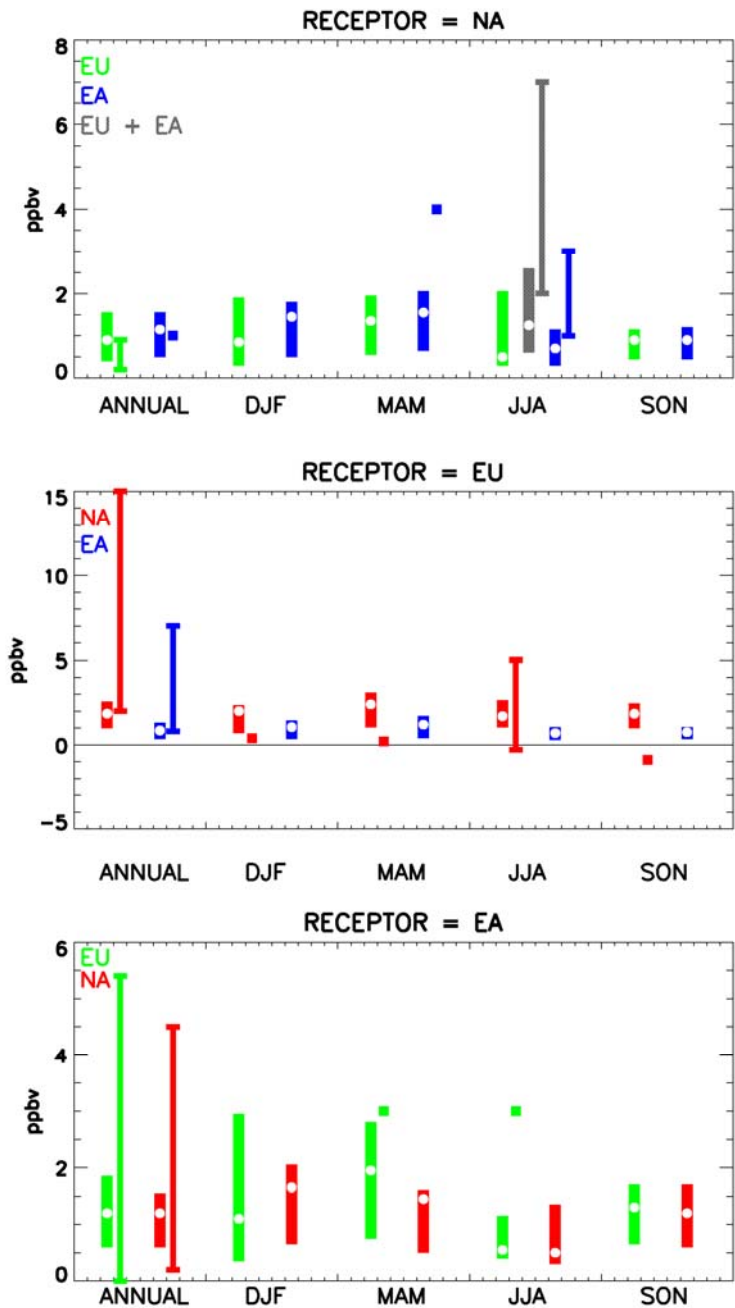
1538
1539
1540
1541
1542
1543
1544
1545

Figure 9. Change in surface O₃ over the EU (left) and NA (right) as a function of various size perturbations to EU anthropogenic NO_x emissions by season (colors), as simulated with the FRSGC/UCI model (solid lines with circles) and as estimated by scaling linearly from the response in the simulation where NO_x emissions were decreased by 20% (SR3EU; dotted lines).



1546
1547
1548
1549
1550
1551
1552

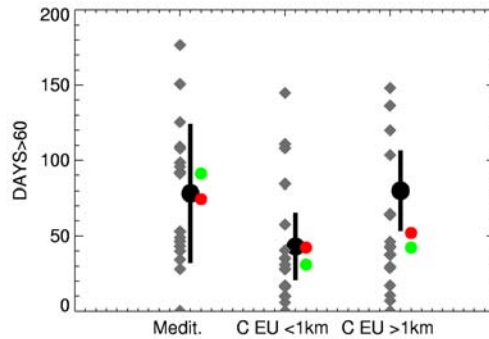
Figure 10. Decrease in annual mean NA surface O₃ (ppb) resulting from 20% reductions in EU anthropogenic NMVOC emissions (SR1-SR4EU) plotted against the EU anthropogenic NMVOC emissions (Tg C a⁻¹). The points represent the results from individual models (EU NMVOC emissions are given in Table A3). The coefficient of determination (r^2) is 0.50.



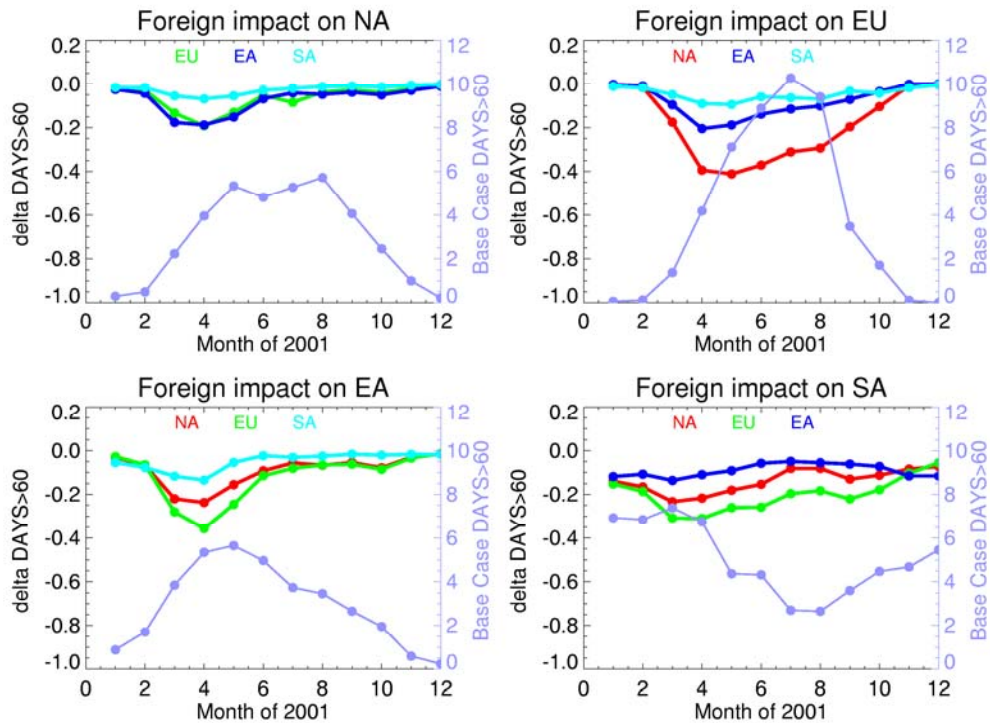
1553
 1554
 1555
 1556
 1557
 1558
 1559
 1560
 1561
 1562
 1563

Figure 11. Annual and seasonal mean contribution to total surface O₃ from foreign source regions as estimated from the individual model results in this study (colored by source region: green for EU; blue for EA, grey for EA+EU; red for NA) and from studies in the published literature (thin vertical bars for range across studies and regions; squares where one value is reported; note that regional definitions, methods for source attribution, and reported metrics (e.g. 24-hour vs. afternoon vs. daytime mean) vary across studies) [Derwent *et al.*, 1998; Berntsen *et al.*, 1999; Wild and Akimoto, 2001; Derwent *et al.*, 2002; Fiore *et al.*, 2002b; Jaeglé *et al.*, 2003; Li *et al.*, 2002; Liu *et al.*, 2002; Pochanart

1564 *et al.*, 2003; *Derwent et al.*, 2004; *Wild et al.*, 2004; *Auvray and Bey*, 2005; *Guerova et*
 1565 *al.*, 2006; *Sudo and Akimoto*, 2007; *Duncan et al.*, 2008; *Holloway et al.*, 2008; *Lin et al.*,
 1566 2008, with all results scaled to 100% contributions as in Table 5-2 of *TF HTAP*, 2007].
 1567 The contributions from this work are estimated by linearly scaling the simulated surface
 1568 O₃ response to the combined 20% decreases in anthropogenic emissions of NO_x, CO, and
 1569 NMVOC in the foreign source regions to 100% decreases, *i.e.*, 5*(SR1-SR6). The white
 1570 circles represent the multi-model median value.
 1571
 1572



1573
 1574 **Figure 12:** Observed (black circles) and simulated (grey diamonds) annual number of
 1575 days when daily maximum 8-hour average O₃ concentrations exceed 60 ppb at the EMEP
 1576 stations, averaged over the regions in Figure 2: Mediterranean (Medit.), Central European
 1577 sites below 1 km altitude (C EU < 1km) and above 1 km altitude (C EU > 1km). The
 1578 black vertical bars depict the standard deviation of the observed values across the stations
 1579 within the region. The model ensemble mean (red circles) and median (green circles)
 1580 values from the 18 models that contributed hourly surface O₃ results for SR1 are also
 1581 shown.



1582
 1583
 1584
 1585
 1586
 1587
 1588
 1589

Figure 13. As in Figure 6 but for the model ensemble mean change in the number of days per month when daily maximum 8-hour average O₃ concentrations exceed 60 ppb, spatially averaged within each receptor region (panels). The change is estimated by first calculating the area-weighted spatial average value for DAYS>60 in each model simulation for a given region (the right axis shows DAYS>60 in the base case, SR1), and then taking the multi-model average of the differences in the spatial average DAYS>60 values (SR6-SR1) from the 12 models that provided hourly surface O₃ results for SR6.